GEÇİCİ KAPAK

Kapak tasarımı
devam ediyor.

BİDGE Yayınları

Advances in Modern Chemistry: From Molecular Structures To Functional Applications

Editör: HÜLYA ÇELİK

ISBN: 978-625-5057-89-1

1. Baskı
Sayfa Düzeni: Gözde YÜCEL
Yayınlama Tarihi: 2026-10-25
BİDGE Yayınları

Bu eserin bütün hakları saklıdır. Kaynak gösterilerek tanıtım için yapılacak kısa alıntılar dışında yayıncının ve editörün yazılı izni olmaksızın hiçbir yolla çoğaltılamaz.

Sertifika No: 71374
Yayın hakları © BİDGE Yayınları
www.bidgeyayinlari.com.tr - bidgeyayinlari@gmail.com
Krc Bilişim Ticaret ve Organizasyon Ltd. Şti.
Güzeltepe Mahallesi Abidin Daver Sokak Sefer Apartmanı No: 7/9 Çankaya / Ankara

PREFACE

Chemistry continues to play a central role in scientific and technological progress, contributing to advances in materials science, pharmaceutical research, environmental applications, and industrial technologies. The growing integration of different chemical disciplines has created new opportunities for understanding molecular properties and developing innovative solutions to contemporary challenges.

This book, Advances in Modern Chemistry: From Molecular Structures to Functional Applications, brings together scientific contributions reflecting recent developments and interdisciplinary approaches in chemical sciences.

The chapters address various aspects of modern chemistry, including the utilization of essential oils in polymeric food packaging, the photodynamic and photothermal antibacterial properties of metal-organic frameworks, and the chemical, structural, and pharmaceutical characteristics of lidocaine. These topics highlight the importance of molecular structure, chemical characterization, and functional properties in scientific research and practical applications.

By presenting contemporary research perspectives, this volume aims to contribute to the exchange of scientific knowledge and encourage further interdisciplinary investigations. It is expected to serve as a valuable resource for researchers, academics, graduate students, and professionals working in chemistry and related fields.

I would like to express my sincere gratitude to all contributing authors for their valuable scientific contributions. I also extend my appreciation to the publisher and everyone involved in the preparation and publication of this book.

I hope that this volume will inspire new research directions and contribute to future advances in chemical sciences.

Prof. Dr. Hülya Çelik

Editor

İÇİNDEKİLER

PHOTODYNAMIC AND PHOTOTHERMAL ANTIBACTERIAL ACTIVITY OF METAL-ORGANIC FRAMEWORKS 1

MELDA İŞLER BİNAY

LIDOCAINE: AROMATIC STRUCTURE, SYNTHESIS, STRUCTURE–ACTIVITY RELATIONSHIPS, AND PHARMACEUTICAL SIGNIFICANCE 25

MUHAMMED EMİN ÇELİK, HÜLYA ÇELİK

UTILIZATION OF ESSENTIAL OILS IN POLYMERIC FOOD PACKAGING 45

ZEHRA KURU, MEHMET ARİF KAYA

BÖLÜM 1

PHOTODYNAMIC AND PHOTOTHERMAL ANTIBACTERIAL ACTIVITY OF METAL ORGANIC FRAMEWORKS

MELDA İŞLER BİNAY[1]

Introduction

Recently, many bacterial infections have been responsible for lethal consequences for living beings (Doan et al., 2025; Doron & Gorbach, 2008; Dridi et al., 2024; Potter, 2001). Multidrug-resistant bacteria constitute a significant part of these pathogenic bacteria (Han et al., 2022; Pettinari et al., 2021). Antimicrobial resistance (AMR) is substantial global health burden, weakening the effectiveness of therapies long central to treating bacterial infections (Pettinari et al., 2021). Bacterial AMR was linked to 4.71 million deaths worldwide in 2021, including 1.14 million directly related to resistance (Naghavi et al., 2024). According to a more recent World Health Organization (WHO) estimate, about one in six laboratory-confirmed bacterial infections responsible for common human infections worldwide were resistant to antibiotic treatment in 2023. Resistance rose in over 40% of monitored pathogen–antibiotic

[1] Dr., Bilkent Üniversitesi, Ulusal Nanoteknoloji Araştırma Merkezi (UNAM), Orcid: 0000-0002-7483-3000

combinations from 2018 to 2023, demonstrating the ongoing loss of effective treatment options (WHO, 2025). By 2050, annual deaths linked to bacterial AMR are projected to reach 8.22 million, including 1.91 million deaths attributable to resistance (Naghavi et al., 2024).

The WHO classified carbapenem-resistant *Acinetobacter baumannii* and *Pseudomonas aeruginosa* as critical-priority pathogens in 2017 because of their clinical importance and capacity to cause healthcare-associated infections (WHO, 2024). Methicillin-resistant Staphylococcus aureus (MRSA) is also considered a high-priority pathogen because of its prevalent occurrence and ability to cause persistent infections involving the skin, soft tissues, bloodstream, lungs, and medical implants. Although the WHO revised its priority pathogen list in 2024, *A. baumannii, P. aeruginosa,* and *S. aureus* continue to pose possible risks to human health (WHO, 2024). In the United States, the Centers for Disease Control and Prevention (CDC) reports more than 2.8 million antimicrobial-resistant infections and over 35,000 deaths each year. Under the CDC's classification, carbapenem-resistant *Acinetobacter* is considered a critical threat, whereas MDR *P. aeruginosa* and MRSA are categorized as serious threats (CDC, 2025)

Although conventional antibiotics are still backbone of treating bacterial infections, many limitations reduce their overall effectiveness. Uncontrolled use can promote the selection of resistant bacterial subpopulations through processes including drug inactivation, target modification, decreased membrane permeability, active efflux, and biofilm formation. At the same time, new antibiotic development has failed to keep pace with the rate at which resistance emerges and spreads. Using high systemic doses can also lead to off-target toxicity, disturb commensal microbial communities, and create selective pressure that encourages resistant strains. Resistance does not follow a fixed one-to-three-year timeline; nonetheless,

resistant phenotypes can appear soon after an antibiotic enters widespread clinical use, especially when therapy targets a single molecular mechanism or is used inappropriately. These concerns have increased interest in non-antibiotic antibacterial approaches that rely less on traditional biochemical drug targets.

Light-responsive antibacterial approaches, especially photodynamic therapy (PDT) and photothermal therapy (PTT), are being explored as alternatives or additions to conventional antibiotic treatment. In PDT, light activates a photosensitizer at a suitable wavelength. This activation triggers energy- or electron-transfer processes that produce reactive oxygen species (ROS), such as singlet oxygen, superoxide radicals, hydroxyl radicals, and hydrogen peroxide. These ROS can damage bacterial membranes, proteins, nucleic acids, and other critical cellular structures. Because oxidative injury targets multiple bacterial components rather than a single enzyme or receptor, antimicrobial PDT may be less likely to promote resistance. However, PDT should not be considered completely resistant to bacterial adaptation, as stress-response pathways and sublethal treatment exposure can still influence susceptibility (Cieplik et al., 2018). Antibacterial PDT has shown effectiveness against Gram-positive and Gram-negative bacteria, including antibiotic-resistant strains and biofilm-associated pathogens (Y. Liu, A. J. Zaat, Breukink, & Heger, 2015).

PTT mechanism depends on converting absorbed light, typically near-infrared light, into localized heat. This heat can damage bacterial features such as bacterial membranes, denature proteins, disrupt intracellular structures, and decompose biofilm matrices. PTT process provides control of antibacterial effects in the exposed region. However, overheating can injure nearby healthy tissue, while inadequate heating may not inactivate bacteria effectively. Using PDT and PTT together may help overcome these limitations. Mild photothermal heating can enhance bacterial

membrane permeability and ROS-mediated injury, while ROS production may decrease the temperature or irradiation dose needed for effective bacterial killing. This dual approach is particularly suitable for multidrug-resistant (MDR) infections and biofilms, which antibiotics are often insufficient to eliminate (Naskar & Kim, 2023).

Metal–organic frameworks (MOFs) are attractive materials for PDT, PTT, and combined phototherapeutic antibacterial applications (P et al., 2025). These porous crystalline structures are formed from metal ions or metal-containing clusters linked by organic molecules. Their adaptable architecture allows tuning of pore size, morphology, surface chemistry, composition, biodegradability, and optical behavior. High porosity and large surface areas also enable the encapsulation, adsorption, or covalent incorporation of photosensitizers, photothermal agents, antibiotics, catalytic species, and targeting ligands. As a result, MOFs can function not only as carriers but also as multifunctional nanoplatforms that combine therapeutic loading, bacterial targeting, stimulus responsiveness, and structural stabilization (Han et al., 2022; Pettinari et al., 2021).

In PDT applications, porphyrinic and other photoactive organic ligands may be built directly into the MOF framework. This design can reduce photosensitizer aggregation and enhance ROS production during irradiation. Photosensitizers can also be loaded into MOF pores, where the framework may improve their aqueous dispersibility and promote interactions with bacterial cells (R. Wang et al., 2023). For PTT, MOFs can incorporate or be combined with photothermal materials, including conductive polymers, carbon-based materials, transition-metal species, and near-infrared-absorbing dyes. Their composition may also include antibacterial metal ions, such as Zn^{2+}, Cu^{2+}, Ag^{+}, or Co^{2+}. These ions can kill bacteria through ion release, membrane damage, oxidative stress, or

disruption of enzymatic activity. MOFs therefore provide an opportunity to combine photodynamic, photothermal, chemodynamic, ion-mediated, and drug-delivery effects within one platform (Han et al., 2022; Matlou & Abrahamse, 2022).

Under light irradiation, MOF-based systems can simultaneously generate ROS and heat to destroy bacteria and disrupt biofilms. Despite this development, several problems must be reconsidered before clinical translation becomes feasible. These include metal ion toxicity, biodegradation, light penetration, bacterial selectivity, and reproducible large-scale synthesis. Current research shows that MOF-based systems can produce ROS and heat at the same time under near-infrared irradiation, improving bacterial eradication and biofilm disruption. Despite this progress, several issues entail further evaluation before clinical translation is feasible. These include biosafety, metal-ion toxicity, colloidal stability, biodegradation, light penetration, bacterial selectivity, and reproducible large-scale synthesis.

This review highlights advances in MOF-derived photodynamic and photothermal antibacterial systems. It covers the mechanisms of photodynamic and photothermal antibacterial processes, design of photoactive MOFs, dual PDT/PTT therapies, and their effectiveness against MDR bacteria. The review further focuses on the challenges for the advancement of MOF-based materials toward clinical antibacterial applications.

Fundamentals of Photodynamic and Photothermal Therapy

Photodynamic therapy (PDT)

In PDT, light activation requires three elements: a photosensitizer (PS), light at an appropriate wavelength, and molecular oxygen (Dolmans et al., 2003). Photon absorption promotes the PS from its ground state (S_0) to an excited singlet state (S_1). From this state, the PS may return to the ground state through

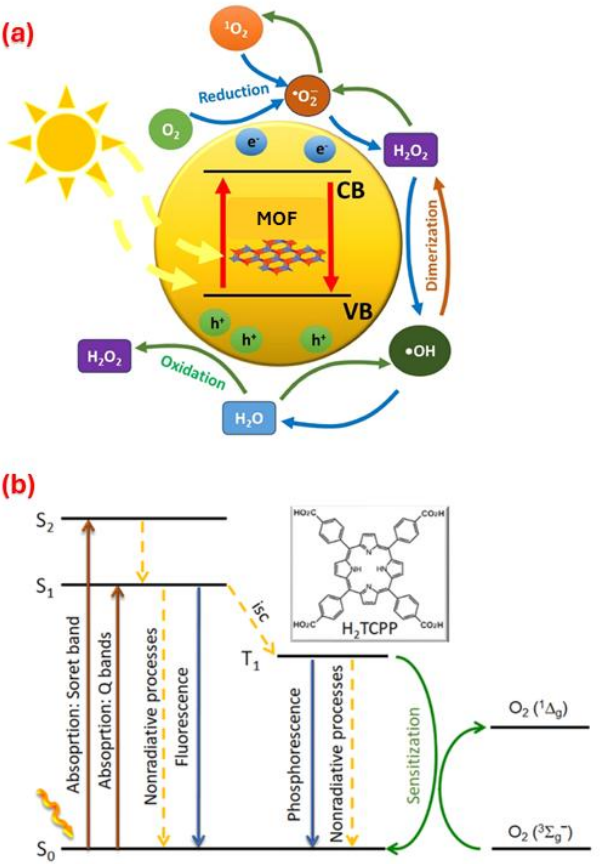
fluorescence emission or heat release. Alternatively, it may undergo intersystem crossing (ISC) and enter a longer-lived excited triplet state (T_1). Because this triplet state persists long enough for the PS to react with nearby substrates, it is primarily responsible for photochemical activity (Castano et al., 2004; Dolmans et al., 2003).

Two reaction routes can originate from the PS triplet state (Figure 1). In the Type I pathway, the PS directly reacts with a biological substrate through electron or hydrogen transfer, producing radical species. These radicals then react with oxygen and generate reactive oxygen species (ROS), including superoxide ($O_2^{\bullet -}$), hydrogen peroxide (H_2O_2), and hydroxyl radical (•OH) (Castano et al., 2004; Hamblin, 2016). In the Type II pathway, energy is transferred from the triplet PS directly to ground-state molecular oxygen ($^3O_2$), producing highly reactive singlet oxygen ($^1O_2$) (Castano et al., 2004; Dolmans et al., 2003). Both pathways can take place simultaneously, with their relative contributions determined by the PS, substrate, and local oxygen concentration. In most MOF-based PDT systems, Type II is the predominant route because the organized porous frameworks position PS linkers or encapsulated PSs to support efficient energy transfer to oxygen.

PDT deactivates bacteria by inducing ROS-mediated oxidative damage to multiple cellular components. The short lifetimes and restricted diffusion distances of $^1O_2$ and •OH in biological media—nanoseconds and tens of nanometers, respectively—mean that the resulting damage occurs close to the PS (Hamblin, 2016). ROS can peroxidize membrane lipids, oxidize proteins and enzymes, and induce DNA strand breaks and base modifications. These combined effects disrupt membrane integrity and ultimately cause cell death (Hamblin, 2016; Wainwright et al., 2017). Since this mechanism affects several targets rather than a single one, bacteria are unlikely to develop resistance. This

represents a key advantage of PDT over conventional antibiotics (Wainwright et al., 2017).

Figure 1 The pathways of the ROS mechanisms. Type I: The generation of superoxide (O_2•$^-$), hydrogen peroxide (H_2O_2), and hydroxyl radical (•OH) (a) and Type II: The generation of singlet oxygen ($^1O_2$) (b).

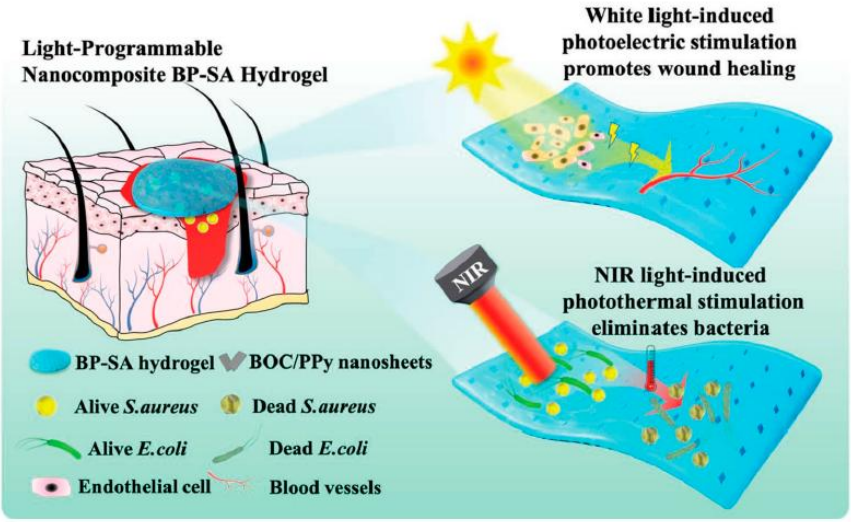


References: (Karousis & Tasis, 2024; Schlachter et al., 2021).

Photothermal therapy (PTT)

Photothermal therapy is the process in which a photothermal agent (PTA) transforms light into heat under light irradiation and inhibits pathogens thermally by destroying bacterial cells and deactivating proteins and DNA of bacteria (He et al., 2021; X. Liu et al., 2021; Yang et al., 2018; Zhao et al., 2023).

Figure 2 The illustration of PTT mechanism of BP-SA.



Reference: (Z. Zhang et al., 2023)

PTT relies on the PTAs that transform absorbed light into heat. Upon light absorption, usually in the near-infrared (NIR) region, electrons in a PTA become excited. They generally return to the ground state through non-radiative relaxation, emitting energy as vibrations (phonons) that increase the temperature of the surrounding medium (X. Chen et al., 2025; Jaque et al., 2014). In plasmonic nanomaterials, a similar process results from the decay of localized surface plasmon resonance. Bacterial damage begins when the local temperature goes beyond approximately 42 °C. More

intense and irreversible injury occurs at higher temperatures, while duration of exposure also influences the outcome (Jaque et al., 2014). Hyperthermia denatures membrane proteins and enzymes, increases membrane fluidity and permeability, and compromises membrane integrity. As cellular contents leak out, cell death eventually follows (X. Chen et al., 2025; L. He et al., 2023). Because heat is produced locally and causes physical damage, PTT is also expected to have low potential to promote resistance. For example, Figure 2 schematically illustrates the antibacterial mechanism of a sodium alginate nanocomposite hydrogel loaded with BiOCl/polypyrrole (i.e., BP-SA) (Z. Zhang et al., 2023).

PTT works at NIR light between 700 and 1100 nm. In this range, hemoglobin, water, and melanin in wounds absorb and scatter light weakly. This allows light to penetrate deeper into tissue while protecting adjacent, uninjured wound tissue. (X. Chen et al., 2025; Smith, Mancini, & Nie, 2009). This feature is especially advantageous for deep-seated and implant-associated infections.

Comparison of PDT and PTT

Although PDT and PTT operate through different mechanisms and have distinct requirements, their respective advantages complement one another. Consequently, many MOF-based platforms integrate both approaches (Table 1).

PDT is constrained by its dependence on oxygen, which is often deficient in biofilms and infected tissues. Although PTT is oxygen-independent, the heat generated during treatment may damage healthy tissue, particularly because bacterial eradication within biofilms generally requires relatively high temperatures.

Table 1 The Comparison of PDT and PTT.

Aspect	PDT	PTT	References
Mechanism	Uses photosensitizers (PS) and light to generate ROS	Uses photothermal agents to convert light energy into heat	(de Matos et al., 2025; Fang et al., 2025)
Dependency on Oxygen	Requires oxygen;	Does not require oxygen	(de Matos et al., 2025)
Therapeutic Effect	Induces oxidative stress causing apoptosis and ROS-mediated cell death	Causes local hyperthermia causing protein denaturation and cell ablation	(Fang et al., 2025; Hou et al., 2020)
Light Source Requirements	Uses specific wavelengths activating PS (e.g., 670 nm)	Uses (NIR) light (e.g., 808 nm) for deeper penetration	(Fang et al., 2025; D. Zhang et al., 2015)
Selectivity and Targeting	Targeting via photosensitizer accumulation; limited by oxygen diffusion	Selectivity through targeted photothermal agents	(Chen & Tang, 2025; Song et al., 2022)
Side Effects and Toxicity	Minimal toxicity to healthy tissue; ROS can cause local damage	Minimal trauma and side effects; localized thermal effect reduces systemic toxicity	(Chen & Tang, 2025; de Matos et al., 2025)
Limitations	Limited tissue penetration due to oxygen dependence	Localized heat distribution; risk of damaging adjacent healthy tissue at high temperatures	(Chen & Tang, 2025; de Matos et al., 2025)

Combination PTT and PDT can lessen these limitations. Insignificant hyperthermia may enhance membrane permeability, local blood flow, and oxygen supply, thereby increasing ROS-mediated killing. Consequently, effective treatment may be achieved

at lower temperatures, reducing damage to healthy tissue (L. He et al., 2023; Smith et al., 2009). Such complementary effects have increased interest in MOFs as multifunctional platforms for combined PDT/PTT.

PDT-Active Antibacterial MOFs Intrinsic Photosensitizer MOFs

PDT-active MOFs may act as intrinsic photosensitizers, undergo post-synthetic modification to enhance photophysical properties, or protect externally introduced photosensitizers as carrier platforms (Matlou & Abrahamse, 2022). Among intrinsic photosensitizing MOFs, porphyrin-containing frameworks have been studied most extensively. Porphyrin ligands show strong visible-light absorption, high molar extinction coefficients, and a natural capacity to access triplet excited states. When periodically fixed within a crystalline framework, porphyrin aggregation and self-quenching are also reduced, which supports maintaining photosensitizing activity (Schlachter et al., 2021).

Porphyrinic zirconium frameworks from the PCN family, such as PCN-224, combine stable Zr_6 clusters with tetrakis(4-carboxyphenyl)porphyrin (TCPP) linkers that serve as built-in photosensitizers (Luo et al., 2021). Under visible-light exposure, the porphyrin units transfer energy to molecular oxygen, producing singlet oxygen ($^1O_2$), which can oxidatively damage bacterial membranes, proteins, and nucleic acids. The high surface area and open porosity of PCN-224 can also support oxygen diffusion, promoting ROS production at the bacteria–material interface. (Bůžek et al., 2021; Q. Liu et al., 2026). The photodynamic activity of PCN-224 can be further enhanced by modifying its metal cluster. In PCN-224(Zr/Ti), partially substituting Zr^{4+} with Ti^{4+} facilitates electron transfer from the excited porphyrin linker to the metal cluster. This process reduces electron–hole recombination and

increases ROS generation. Recent antimicrobial-MOF literature has reported particularly strong activity of PCN-224(Zr/Ti) against multidrug-resistant pathogens, including methicillin-resistant *S. aureus* (MRSA), *E. coli*, and *A. baumannii* (Q. J. Li et al., 2025). This strategy underlines that adjusting the inorganic node can extend the lifetime of photoexcited charge carriers without altering the porphyrin photosensitizer itself.

Similar research has been carried out with hafnium-porphyrin MOFs (Matlou & Abrahamse, 2022). In Hf-containing porphyrinic MOFs, the heavy Hf center may increase intersystem crossing of an excited photosensitizer to its triplet state through the heavy-atom effect. This process can improve energy transfer to oxygen and thereby increase $^1O_2$ production. Hf–TCPP and related Hf porphyrinic frameworks have therefore been investigated as intrinsically photoactive MOFs with high photosensitizer loading, considerable porosity, and improved ROS generation. Although these materials have primarily been studied for cancer PDT, the same photophysical mechanism also applies to antimicrobial photodynamic therapy (Matlou & Abrahamse, 2022).

Fe^{3+}-containing MOFs provide an alternative antibacterial route through Fenton or photo-Fenton chemistry. Iron centers react with hydrogen peroxide to form highly oxidative radical species, particularly hydroxyl radicals, while visible-light excitation can improve charge separation and support redox cycling between iron oxidation states (Du et al., 2022). Fe-MOFs are therefore useful where endogenous or externally supplied H_2O_2 is available, including infected and inflamed tissues. Their photocatalytic performance depends on the electronic properties of Fe–oxo clusters, the linker's light-absorption behavior, and the framework's ability to retain accessible iron sites while limiting excessive metal leaching. Although photo-Fenton research has largely focused on

environmental catalysis, its core principles can be adapted for antibacterial platforms that increase localized oxidative stress (Du et al., 2022).

ZIF-8 is a zinc-based framework formed from Zn^{2+} and 2-methylimidazolate linkers. Its antibacterial effects are commonly linked to Zn^{2+} release, and photoinduced ROS production. Through ligand-to-metal charge transfer, photogenerated electrons can accumulate at Zn centers, supporting oxygen reduction and ROS formation (Zou et al., 2023). Nevertheless, unmodified ZIF-8 absorbs visible light weakly. High photodynamic performance therefore often depends on defect engineering, heterojunction construction, sensitizer loading, or integration with light-harvesting nanomaterials (Zou et al., 2023).

Post-synthetic modification gives a practical way to increase ROS production while preserving the MOF's original structural benefits. Depositing Ag nanoparticles on porphyrinic MOFs is one such approach. Silver provides direct ion-mediated antibacterial effects, whereas its plasmonic properties can strengthen local electromagnetic fields and improve charge separation during irradiation (X. Li et al., 2022). In Ag-decorated Co-TCPP MOF nanosheets, 660 nm irradiation produced $^1O_2$ and supported sustained Ag^+ release, resulting in combined photodynamic and silver-ion antibacterial activity (X. Li et al., 2022).

Porphyrinic-MOF photodynamic behavior can also be improved with graphene or carbon quantum dots. In a bacterial-cellulose/CQD@PCN-224 membrane, fluorescence resonance energy transfer from carbon quantum dots to PCN-224 enhanced the photodynamic response of the porphyrin framework (Wang et al., 2023). After 30 min of visible-light exposure, the membrane achieved greater than 99.99% reduction of both *S. aureus* and *E. coli*

O157:H7. This design shows how an antenna component can improve or expand light harvesting while PCN-224 remains the main $^1O_2$-producing photosensitizer (Wang et al., 2023).

MOFs as Carriers for External Photosensitizers

MOFs can stabilize, disperse, and localize photosensitizers that tend to aggregate, have low aqueous stability, or undergo early photobleaching (Songca, 2024; Tao, Yuan, & Zhou, 2026; Yutao Zou, Zhang, Chen, Wang, & Zheng, 2025). Indocyanine green (ICG), known as a photosensitizer due to its capability of absorbing NIR light, was loaded into Fe- or Al-based MOFs, including Fe-101-, Al-101-, and Fe-88-type hosts (Yutao Zou et al., 2025). This process minimized dye aggregation and improved storage stability. Under NIR irradiation, these systems may generate ROS and heat simultaneously, promoting antibacterial activity while leveraging NIR light's deeper penetration (Yutao Zou et al., 2025).

Encapsulating squaraine (SQ) dyes in ZIF-8 is a related strategy (Lemmens & Pal, 2019). Charge transfer from excited SQ to the ZIF-8 framework can prolong the dye triplet-state lifetime and enhance $^1O_2$ production. In infection-associated acidic environments, ZIF-8 degradation may also release Zn^{2+}, producing combined oxidative and metal-ion antibacterial activity. The key advantage is that the MOF acts as both a dye carrier and a pH-responsive antibacterial co-agent (Lemmens & Pal, 2019).

PTT-Active Antibacterial MOFs

Photothermal therapy (PTT) transforms absorbed light into localized heat. At antibacterial temperatures, heat can destabilize membranes, denature proteins, disrupt metabolic pathways, and weaken biofilm matrices. MOF-based PTT platforms are generally created through incorporating photothermal inorganic phases,

carbonizing MOFs into carbonaceous derivatives, or using inherently photothermal coordination frameworks such as Prussian blue (Dacarro & Taglietti, 2018).

Partial in situ sulfuration of copper MOFs can efficiently convert Cu-containing framework regions into photothermal CuS nanoparticles (Yu et al., 2020). In CuS@HKUST-1, Cu sites within HKUST-1 are partially transformed into CuS nanodomains, while the MOF-derived structure remains as a support. CuS shows strong NIR absorption and can rapidly convert light into heat via localized surface plasmon resonance (Yu et al., 2020). After 20 min of NIR irradiation, CuS@HKUST-1 reportedly achieved inactivation rates of 99.70% for *S. aureus* and 99.80% for *E. coli*. Its antibacterial activity was attributed to combined photothermal and photocatalytic effects. NIR excitation in this system generates heat, while photogenerated charge carriers may also support ROS formation, including •OH under appropriate aqueous conditions. Rather than acting only as a passive scaffold, the framework spatially confines CuS nanophases and supports an integrated PTT/PDT mechanism.

Pyrolysis of MOFs offers porous carbon materials with dispersed metal or metal-oxide species. ZIF-8, having Zn-containing nodes and nitrogen-rich imidazolate linkers, is particularly useful as a precursor to form ZnO-containing carbon or Zn-doped graphitic carbon, depending on the pyrolysis atmosphere and temperature (Zheng et al., 2024). Adding Ag^{+} introduced a further ion-mediated antibacterial effect. Studies of Ag-containing ZIF-8-derived porous carbon indicate that atomically dispersed Ag may enhance NIR absorption and photothermal performance while also contributing antibacterial activity against *S. aureus* and *E. coli*. These multifunctional materials should therefore be described as combining heat, residual Zn-containing species, and Ag-associated

antibacterial effects rather than as PTT-only systems (Zheng et al., 2024).

Prussian blue, represented as $Fe_4[Fe(CN)_6]_3$, is a recognized photothermal metal-organic framework with strong NIR absorption, often used at 808 nm (Dacarro & Taglietti, 2018). Its photothermal behaviour is driven by intervalence charge transfer followed by efficient non-radiative relaxation. In antimicrobial systems, Prussian blue can provide localised heat and also function as a core for heterostructured MOF assemblies (Dacarro & Taglietti, 2018). Zn^{2+}-doped Prussian blue MOFs have been suggested as a means to improve photothermal performance while introducing metal-ion antibacterial activity (J. Li et al., 2019). Replacing Fe–CN–Fe linkages with Fe–CN–Zn can modify lattice defects and electronic properties, possibly shifting absorption towards longer wavelengths and raising photothermal conversion. During NIR heating, Zn^{2+} release may also be accelerated, allowing thermal damage to occur alongside zinc-mediated disruption of bacterial membranes and metabolism. This design may be useful for infected wounds, where local illumination could provide spatial control of heat production and ion delivery (J. Li et al., 2019).

In 2022, Ma et al. reported Cu-MOF nanosheets with Cu^{2+} as the central ion and tetrakis(4-carboxyphenyl)porphyrin (TCPP) as the ligand. These two-dimensional nanosheets were altered with manganese dioxide. In this system, Cu^{2+} and MnO_2 constituents react with intracellular GSH and hydrogen peroxide to form hydroxyl radicals via a Fenton-like reaction. Additionally, Cu^{2+} can undergo a Russell reaction to produce cytotoxic singlet oxygen (Ma et al., 2022).

Dual PDT/PTT Synergistic MOF Systems

PDT/PTT systems combine oxidative stress and heat so each can strengthen the other's effects. PTT-induced hyperthermia can damage bacterial membranes and biofilm matrices, increasing ROS penetration and intracellular susceptibility. In turn, ROS generated during PDT may impair heat-shock defenses, membrane-repair pathways, and respiratory processes, making bacteria less tolerant of hyperthermia. Heat may also enhance mass transfer and support diffusion of ROS or released antimicrobial ions through biofilms (Naskar & Kim, 2023).

In the literature, the PB@PCN-224 heterojunction, where a Prussian blue core provides photothermal conversion and a PCN-224 porphyrinic shell provides photodynamic activity, was designed (Luo et al., 2021). Under 660 nm irradiation, interfacial electron transfer is promoted within the heterojunction, delaying electron–hole recombination and enhancing ROS generation compared with the individual components. Simultaneously, the Prussian blue phase produces photothermal heat. Reported antibacterial efficiencies were 99.84% against planktonic *S. aureus* and 99.3% against *S. aureus* biofilms after 15 min of irradiation (Luo et al., 2021). The PB@PCN-224 platform also illustrates a broader principle: heterojunction engineering can improve performance by altering charge-transfer behavior, not simply by combining two active materials. Here, the porphyrin framework separates photogenerated electrons, while the Prussian blue phase provides the photothermal route. Together, these components unite charge management, ROS generation, and heat production within a single structure (Luo et al., 2021).

Fe–porphyrin MOF, an Au@MOF core–shell hybrid material, offers another possible multimodal platform (Cai et al.,

2021). The porphyrin linker may generate $^1O_2$ through PDT, while Fe centers can take part in Fenton-like reactions that produce •OH in the presence of H_2O_2. Extensive adsorption at 650 nm via Au nanorods generates the PTT effect. A third mechanism, photothermal heating, may be added if the framework or an incorporated component exhibits strong non-radiative relaxation. Such systems may be particularly relevant in infected tissues with elevated oxidative stress, although their performance will depend on local H_2O_2 concentration, oxygen availability, light penetration, and stable Fe redox cycling (Cai et al., 2021).

Conclusions and Future Perspectives

Metal–organic frameworks (MOFs) deliver promising solutions for advanced bacterial inhibition technologies through photodynamic therapy (PDT) and photothermal therapy (PTT). The intrinsic antibacterial activity of metal nodes and tunable porosity, which enables encapsulation of photosensitizers and/or antibiotics, make MOFs preferable for antibacterial applications. In PDT, light-sensitive MOFs produce reactive oxygen species that damage bacterial cellular components, while in PTT, MOF systems convert absorbed light into heat, disrupting membranes and degrading proteins.

Still, many challenges prevent MOF-derived systems from clinical use. Release of metal content and degradation into byproducts could result in toxicity. Moreover, limited light penetration reduces PTT efficacy, while exaggerated PTT-induced heating may damage healthy tissues. Additional challenges comprise limited oxygen access for PDT, which reduces selectivity for bacteria over host cells, and difficulty attaining reproducible large-scale synthesis.

References

Bůžek, D., Adamec, S., Lang, K., & Demel, J. (2021). Metal-organic frameworks: Vs. buffers: Case study of UiO-66 stability. *Inorganic Chemistry Frontiers*, *8*(3), 720–734. https://doi.org/10.1039/d0qi00973c

Cai, X., Zhao, Y., Wang, L., Hu, M., Wu, Z., Liu, L., Zhu, W., & Pei, R. (2021). Synthesis of Au@MOF core–shell hybrids for enhanced photodynamic/photothermal therapy. *Journal of Materials Chemistry B*, *9*(July), 6646–6657. https://doi.org/10.1039/d1tb00800e

Castano, A. P., Demidova, T. N., & Hamblin, M. R. (2004). Mechanisms in photodynamic therapy: part one—photosensitizers, photochemistry and cellular localization. *Photodiagnosis Photodyn. Ther.*, *1*(4), 279–293. https://doi.org/10.1016/S1572-1000(05)00007-4.

Chen, Y., & Tang, D. (2025). Precision nanomaterials in colorectal cancer: advancing photodynamic and photothermal therapy. *RSC Advances*, *15*(33), 26583–26600. https://doi.org/10.1039/d5ra03996g

Dacarro, G., & Taglietti, A. (2018). Prussian Blue Nanoparticles as a Versatile Photothermal Tool. *Molecules*, *23*(1414), 1–20. https://doi.org/10.3390/molecules23061414

de Matos, P. A., de Oliveira, H. C. N., da Silva, M. N. T., Nossol, E., & Tsubone, T. M. (2025). Metal hexacyanoferrates in photodynamic and photothermal therapies. *Biophysical Reviews*, *17*(2), 561–577. https://doi.org/10.1007/s12551-025-01287-w

Doan, T. D., Vu, N. N., Hoang, T. L. G., & Nguyen-Tri, P. (2025). Metal-organic framework (MOF)-based materials for photocatalytic antibacterial applications. *Coordination Chemistry Reviews*, *523*, 216298. https://doi.org/10.1016/j.ccr.2024.216298

Dolmans, D. E. J. G. J., Fukumura, D., & Jain, R. K. (2003). Photodynamic therapy for cancer. *Nature Reviews Cancer*,

3(5), 375–380. https://doi.org/10.1038/nrc1070

Doron, S., & Gorbach, S. L. (2008). Bacterial Infections: Overview. In P. F. Lewis (Ed.), *International encyclopedia Public Health* (p. 273). https://doi.org/10.1016/B978-0-323-01199-0.50123-7

Dridi, D., Vu, N. N., Singh, J., Eesaee, M., Saidi, A., Elkoun, S., & Nguyen-Tri, P. (2024). Recent advances on engineering of silver related nanocomposites toward antibacterial applications. *Nano-Structures and Nano-Objects*, *38*(June), 101195. https://doi.org/10.1016/j.nanoso.2024.101195

Du, C., Zhang, Y., Zhang, Z., Zhou, L., Yu, G., Wen, X., Chi, T., Wang, G., Su, Y., Deng, F., Lv, Y., & Zhu, H. (2022). Fe-based metal organic frameworks (Fe-MOFs) for organic pollutants removal via photo-Fenton: A review. *Chemical Engineering Journal*, *431*. https://doi.org/10.1016/j.cej.2021.133932

Fang, L., Chen, Z., Dai, J., Pan, Y., Tu, Y., Meng, Q., Diao, Y., Yang, S., Guo, W., Li, L., Liu, J., Wen, H., Hua, K., Hang, L., Fang, J., Meng, X., Ma, P., & Jiang, G. (2025). Recent Advances in Strategies to Enhance Photodynamic and Photothermal Therapy Performance of Single-Component Organic Phototherapeutic Agents. *Advanced Science*, *12*(7), 1–30. https://doi.org/10.1002/advs.202409157

Hamblin, M. R. (2016). Antimicrobial photodynamic inactivation: a bright new technique to kill resistant microbes Kill Resistant Microbes. *Current Opinion in Microbiology*, *33*, 67–73. https://doi.org/10.1016/j.mib.2016.06.008.Antimicrobial

Han, D., Liu, X., & Wu, S. (2022). Metal organic framework-based antibacterial agents and their underlying mechanisms. *Chemical Society Reviews*, *51*(16), 7138–7169. https://doi.org/10.1039/d2cs00460g

He, W., Wang, Z., Bai, H., Zhao, Z., Kwok, R. T. K., Lam, J. W. Y., & Tang, B. Z. (2021). Highly efficient photothermal nanoparticles for the rapid eradication of bacterial biofilms. *Nanoscale Communication*, *13*(32), 13610–13616. https://doi.org/10.1039/d1nr03471e

Hou, Y. J., Yang, X. X., Liu, R. Q., Zhao, D., Guo, C. X., Zhu, A. C., Wen, M. N., Liu, Z., Qu, G. F., & Meng, H. X. (2020). Pathological mechanism of photodynamic therapy and photothermal therapy based on nanoparticles. *International Journal of Nanomedicine*, *15*, 6827–6838. https://doi.org/10.2147/IJN.S269321

Karousis, N., & Tasis, D. (2024). Porous covalent organic frameworks in photocatalytic ROS-mediated processes. *Energy Advances*, *3*(4), 712–740. https://doi.org/10.1039/d4ya00082j

Li, J., Liu, X., Tan, L., Cui, Z., Yang, X., Liang, Y., Li, Z., Zhu, S., Zheng, Y., Wai, K., Yeung, K., Wang, X., & Wu, S. (2019). Zinc-doped Prussian blue enhances photothermal clearance of Staphylococcus aureus and promotes tissue repair in infected wounds. *Nature Communications*, *10*, 4490.

Li, Q. J., Xing, F., Wu, W. T., Zhe, M., Zhang, W. Q., Qin, L., Huang, L. P., Zhao, L. M., Wang, R., Fan, M. H., Zou, C. Y., Duan, W. Q., Li-Ling, J., & Xie, H. Q. (2025). Multifunctional metal–organic frameworks as promising nanomaterials for antimicrobial strategies. *Burns and Trauma*, *13*. https://doi.org/10.1093/burnst/tkaf008

Li, X., Zhao, X., Chu, D., Zhu, X., Xue, B., Chen, H., Zhou, Z., & Li, J. (2022). Silver nanoparticle-decorated 2D Co-TCPP MOF nanosheets for synergistic photodynamic and silver ion antibacterial. *Surfaces and Interfaces*, *33*(July), 1–8. https://doi.org/10.1016/j.surfin.2022.102247

Liu, Q., Tang, C., Liu, J., Gao, Y., & Peng, L. (2026). Zr-porphyrinic MOF PCN-224 enables sequential antibacterial and inflammation-modulating PDT for periodontitis. *Colloids and Surfaces B: Biointerfaces*, *265*(February). https://doi.org/10.1016/j.colsurfb.2026.115692

Liu, X., Yang, Y., Ling, M., Sun, R., Zhu, M., Chen, J., Yu, M., Peng, Z., Yu, Z., & Liu, X. (2021). Near-Infrared II Light-Triggered Robust Carbon Radical Generation for Combined Photothermal and Thermodynamic Therapy of Hypoxic Tumors. *Advanced Functional Materials*, *31*(24), 1–15.

https://doi.org/10.1002/adfm.202101709

Luo, Y., Liu, X., Tan, L., Li, Z., Wai, K., Yeung, K., & Zheng, Y. (2021). Enhanced photocatalytic and photothermal properties of ecofriendly metal-organic framework heterojunction for rapid sterilization. *Chemical Engineering Journal*, *405*, 1236730. https://doi.org/https://doi.org/10.1016/j.cej.2020.126730

Ma, W., Zhang, H., Li, S., Wang, Z., Wu, X., Yan, R., Geng, F., Mu, W., & Jin, Y. (2022). A Multifunctional Nanoplatform Based on Fenton-like and Russell Reactions of Cu , Mn Bimetallic Ions Synergistically Enhanced ROS Stress for Improved Chemodynamic Therapy. *ACS Biomaterials Science & Engineering*.

Matlou, G. G., & Abrahamse, H. (2022). Nanoscale metal–organic frameworks as photosensitizers and nanocarriers in photodynamic therapy. *Frontiers in Chemistry*, *10*(August), 1–14. https://doi.org/10.3389/fchem.2022.971747

Naghavi, M., Vollset, S. E., Ikuta, K. S., Swetschinski, L. R., Gray, A. P., Wool, E. E., Robles Aguilar, G., Mestrovic, T., Smith, G., Han, C., Hsu, R. L., Chalek, J., Araki, D. T., Chung, E., Raggi, C., Gershberg Hayoon, A., Davis Weaver, N., Lindstedt, P. A., Smith, A. E., … Murray, C. J. L. (2024). Global burden of bacterial antimicrobial resistance 1990–2021: a systematic analysis with forecasts to 2050. *The Lancet*, *404*(10459), 1199–1226. https://doi.org/10.1016/S0140-6736(24)01867-1

Naskar, A., & Kim, K. S. (2023). Friends against the Foe: Synergistic Photothermal and Photodynamic Therapy against Bacterial Infections. *Pharmaceutics*, *15*(4). https://doi.org/10.3390/pharmaceutics15041116

P, E., Durantini, J. E., Milanesio, E., & Durantini, E. N. (2025). BODIPY-Loaded ZIF-8 Nanomaterials for Enhanced Photodynamic Inactivation of Staphylococcus aureus. *Applied Biomaterials*, *8*, 6316–6325.

Pettinari, C., Pettinari, R., Di Nicola, C., Tombesi, A., Scuri, S., &

Marchetti, F. (2021). Antimicrobial MOFs. *Coordination Chemistry Reviews*, *446*. https://doi.org/10.1016/j.ccr.2021.214121

Potter, C. W. (2001). A history of influenza. *Journal of Applied Microbiology*, *91*(4), 572–579.

Schlachter, A., Asselin, P., & Harvey, P. D. (2021). Porphyrin-Containing MOFs and COFs as Heterogeneous Photosensitizers for Singlet Oxygen-Based Antimicrobial Nanodevices. *ACS Applied Materials and Interfaces*, *13*(23), 26651–26672. https://doi.org/10.1021/acsami.1c05234

Song, L., Chen, B., Qin, Z., Liu, X., Guo, Z., Lou, H., Liu, H., Sun, W., Guo, C., & Li, C. (2022). Temperature-Dependent CAT-Like RGD-BPNS@SMFN Nanoplatform for PTT-PDT Self-Synergetic Tumor Phototherapy. *Advanced Healthcare Materials*, *11*(8), 1–16. https://doi.org/10.1002/adhm.202102298

Wainwright, M., Maisch, T., Nonell, S., Plaetzer, K., Almeida, A., Tegos, G. P., & Hamblin, M. R. (2017). Photoantimicrobials—are we afraid of the light? *Lancet Infec. Dis.*, *17*, e49–e55. https://pubmed.ncbi.nlm.nih.gov/33744382/

Wang, Y., Ai, J., Nie, X., Li, Z., Xia, X., Hussain, T., Wang, Q., & Wei, Q. (2023). Photodynamic activity enhanced by in situ biosynthetic BC/CQDs@PCN-224 membranes through FRET strategy. *Carbohydrate Polymers*, *307*(November 2022). https://doi.org/10.1016/j.carbpol.2023.120623

WHO. (2025). *Global antibiotic resistance surveillance report 2025*. https://www.who.int/publications/i/item/9789240116337

Yang, X., Li, H., Qian, C., Guo, Y., Li, C., Gao, F., Yang, Y., Wang, K., Oupicky, D., & Sun, M. (2018). Near-infrared light-activated IR780-loaded liposomes for anti-tumor angiogenesis and Photothermal therapy. *Nanomedicine: Nanotechnology, Biology, and Medicine*, *14*(7), 2283–2294. https://doi.org/10.1016/j.nano.2018.06.011

Zhang, D., Wu, M., Zeng, Y., Wu, L., Wang, Q., Han, X., Liu, X.,

& Liu, J. (2015). Chlorin e6 conjugated poly(dopamine) nanospheres as PDT/PTT dual-modal therapeutic agents for enhanced cancer therapy. *ACS Applied Materials and Interfaces*, *7*(15), 8176–8187. https://doi.org/10.1021/acsami.5b01027

Zhang, Z., Xie, J., Xing, J., Li, C., Wong, T. M., Yu, H., Li, Y., Yang, F., Tian, Y., Zhang, H., Li, W., Ning, C., Wang, X., & Yu, P. (2023). Light-Programmable Nanocomposite Hydrogel for State-Switchable Wound Healing Promotion and Bacterial Infection Elimination. *Advanced Healthcare Materials*, *12*(2), 1–15. https://doi.org/10.1002/adhm.202201565

Zhao, Y., Wang, Y., Wang, X., Qi, R., & Yuan, H. (2023). Recent Progress of Photothermal Therapy Based on Conjugated Nanomaterials in Combating Microbial Infections. *Nanomaterials*, *13*(2269), 1–29.

Zheng, Y., Cai, X., Chen, G., Xiang, D., Shi, W., Shen, J., & Xiang, B. (2024). Single Atom-Dispersed Silver Incorporated in ZIF-8-Derived Porous Carbon for Enhanced Photothermal Activity and Antibacterial Activities. *International Journal of Nanomedicine*, *19*(May), 4253–4261. https://doi.org/10.2147/IJN.S459176

Zou, Y., Weng, J., Qin, Z., Zhang, Y., Ji, S., & Zhang, H. (2023). Metal–organic framework- and graphene quantum dot-incorporated nanofibers as dual stimuli-responsive platforms for day/night antibacterial bio-protection. *Chemical Engineering Journal*, *473*(July). https://doi.org/10.1016/j.cej.2023.145365

BÖLÜM 2

LIDOCAINE: AROMATIC STRUCTURE, SYNTHESIS, STRUCTURE–ACTIVITY RELATIONSHIPS, AND PHARMACEUTICAL SIGNIFICANCE

MUHAMMED EMİN ÇELİK[1]
HÜLYA ÇELİK[2]

Introduction

Local anesthetics reversibly suppress the initiation and propagation of action potentials, principally by reducing sodium conductance through voltage-gated sodium (Na_v) channels. Lidocaine occupies a particularly important position in this class because of its well-characterized local anesthetic properties and its additional use, under specific clinical conditions, as a class Ib antiarrhythmic agent (Becker & Reed, 2012; O'Leary & Chahine, 2018). These actions cannot be attributed to an aromatic ring alone: the ionization state of the amino group, membrane access, protein

[1] Student, Ağrı İbrahim Çeçen University, Faculty of Pharmacy, ORCID: 0009-0000-7332-4119
[2] Prof. Dr., Ağrı İbrahim Çeçen University, Faculty of Pharmacy, Department of Basic Pharmaceutical Sciences, Division of Basic Pharmacy Sciences, ORCID: 0000-0003-0805-0523

binding, channel conformation, systemic distribution, and metabolism must be considered together.

From an organic chemistry perspective, lidocaine combines an aromatic aryl moiety, a polar carboxamide linkage, and a flexible aminoalkyl fragment. These units provide an instructive framework for examining resonance, steric effects, protonation equilibria, nucleophilic acyl substitution, and bimolecular nucleophilic substitution. A chemically informed understanding is also essential for avoiding simplistic conclusions such as equating greater lipophilicity with universally improved efficacy or interpreting structural stability as evidence of clinical safety (Butterworth & Strichartz, 1990).

Chemical Identity and Molecular Architecture

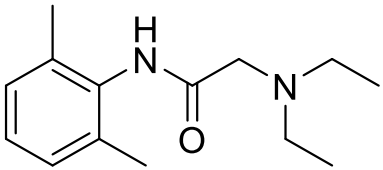
Table 1 summarizes the chemical identity and key structural characteristics of lidocaine, and Figure 1 shows its structural formula.

Table 1 Chemical identity and key structural characteristics of lidocaine

Property	**Description**
Preferred systematic (IUPAC) name	2-(Diethylamino)-N-(2,6-dimethylphenyl)acetamide
CAS Registry Numbers	137-58-6 (free base); 73-78-9 (hydrochloride); 6108-05-0 (HCl monohydrate)
Molecular formula & molar mass (free base)	C14H22N2O (234.34 g mol−1)
Molecular formula & molar mass (HCl salt)	C14H22N2O·HCl·H2O (288.81 g mol−1, hydrochloride monohydrate)
Key structural motifs	Lipophilic 2,6-dimethylphenyl ring; secondary carboxamide linkage; hydrophilic tertiary diethylamino group
Pharmacological classification	Amide-type local anesthetic; Vaughan Williams class Ib antiarrhythmic agent

Source: Prepared by the authors.

Figure 1 Chemical structure of lidocaine (2-(diethylamino)-N-(2,6-dimethylphenyl)acetamide)



Source: Prepared by the authors.

The amide nitrogen is attached to a 2,6-dimethyl-substituted phenyl ring. The ortho methyl groups influence both the electron distribution of the aromatic system and the steric environment around the aryl–amide connection. The carbonyl group provides a strongly polarized C=O bond, while delocalization of the amide nitrogen lone pair toward the carbonyl limits its basicity and restricts rotation about the C–N linkage. In contrast, the terminal diethylamino nitrogen is a protonatable tertiary amine. Thus, neutral and cationic species coexist in proportions determined by environmental pH and the relevant acid dissociation equilibrium (Becker & Reed, 2012).

In pharmaceutical formulations, lidocaine is utilized either as the lipophilic free base ($C_{14}H_{22}N_2O$, 234.34 g mol−1, mp 68–69 °C) for topical, mucosal, and transdermal delivery or as the water-soluble hydrochloride monohydrate salt ($C_{14}H_{22}N_2O{\cdot}HCl{\cdot}H_2O$, 288.81 g mol−1, mp 77–78 °C) for aqueous parenteral and infiltration solutions. Salt formation proceeds via reversible protonation of the terminal tertiary amine to form a diethylammonium cation paired with a chloride counterion, dramatically enhancing aqueous solubility while preserving the covalent pharmacophore. Specifying whether analytical measurements or formulation parameters refer to the free base or the hydrochloride salt is therefore essential for accurate pharmaceutical characterization (National Center for Biotechnology Information, n.d.).

Aromatic Electronic Structure

Hückel aromaticity and resonance

The phenyl ring comprises six sp^2-hybridized carbon atoms whose approximately parallel p orbitals form a continuous cyclic π system. Its six π electrons satisfy Hückel's 4n + 2 relationship for n = 1. Kekulé structures are resonance contributors rather than separate arrangements between which individual double bonds physically alternate. Aromatic delocalization therefore cannot be interpreted as the presence of three chemically isolated alkene groups (Smith & March, 2007).

The two methyl substituents can donate electron density weakly through inductive and hyperconjugative effects and can modify the reactivity of the ring without destroying aromaticity. Aromatic stabilization, however, is not equivalent to overall chemical inertness: processes affecting the amide or aminoalkyl portions may occur with the phenyl ring remaining intact. The distinction between aromatic stabilization and whole-molecule stability is essential to rigorous structural interpretation.

Conjugation and its limits

Electronic communication between the phenyl ring and the carbonyl-bearing moiety occurs through the aryl–NH–C(=O) framework, yet its magnitude is governed by both resonance competition and steric conformation. Because the amide nitrogen lone pair delocalizes predominantly into the adjacent carbonyl group (imparting partial C–N double-bond character and rotational restriction), the aryl-bound nitrogen is markedly less basic and less nucleophilic than the free amino group of 2,6-dimethylaniline. Crucially, the two flanking ortho-methyl substituents impose substantial steric hindrance, forcing the carboxamide plane out of the plane of the benzene ring into a markedly twisted, nearly orthogonal arrangement. This non-coplanar geometry simultaneously

diminishes aryl–amide π-overlap and provides a three-dimensional steric shield around the carbonyl carbon, protecting the amide linkage against rapid enzymatic hydrolysis by plasma esterases and hepatic amidases (Carey & Sundberg, 2007; Smith & March, 2007).

Importantly, the tertiary diethylamino nitrogen is not continuously conjugated with the phenyl π system. The carbonyl–methylene-containing spacer interrupts any uninterrupted p-orbital pathway. It would therefore be misleading to describe this nitrogen as a directly conjugated auxochromic donor to the aromatic ring. Aromatic resonance, substituent polarization, and steric effects should be interpreted as related but distinct phenomena.

Substituent Effects and Potential Aromatic Reactions

Alkyl groups are generally weakly electron-donating and ortho/para-directing in electrophilic aromatic substitution. Nevertheless, the substitution pattern of lidocaine is more complex than that of toluene: two ortho methyl substituents coexist with an amide-linked nitrogen-containing substituent, and steric hindrance can be substantial. Accordingly, the major product of a proposed nitration, halogenation, or sulfonation cannot be predicted with certainty from a single directing rule (Carey & Sundberg, 2007; Smith & March, 2007).

Strongly acidic reagents can also protonate the tertiary amino group and alter the behavior of the functionalized molecule. Reactions theoretically possible on an aromatic ring must be distinguished from experimentally documented preparation of a specific lidocaine derivative. In particular, reactivity observed for free 2,6-dimethylaniline should not be transferred without qualification to the corresponding amide in lidocaine. A reliable regioselectivity claim requires an identified reaction product and supporting analytical evidence. Specifically, because positions C1, C2, and C6 of the phenyl ring are already occupied, only the C3/C5

(meta to the amide, ortho/para to the methyl groups) and C4 (para to the amide, meta to the methyl groups) positions remain available for substitution. Which of these positions would actually react depends on the reagent and conditions and must be established experimentally for each case.

Chromophoric and Spectroscopic Considerations

The phenyl ring is an important ultraviolet chromophore because it supports $\pi \rightarrow \pi^*$ electronic transitions. The amide group contributes additional electronic transitions, although the presence of a benzene ring or carbonyl does not in itself imply strong absorption in the visible region. The spectral approaches commonly used for lidocaine answer different questions: UV–visible spectroscopy probes electronic absorption, IR spectroscopy probes bond vibrations, and nuclear magnetic resonance (NMR) spectroscopy probes atomic magnetic environments (Pavia et al., 2015).

In IR spectra, the amide carbonyl and N–H stretching modes, together with aromatic and aliphatic C–H vibrations, provide useful functional-group evidence. In ^{1}H NMR spectroscopy, the 2,6-disubstituted aromatic ring has three hydrogen atoms; the aromatic resonances can be considered alongside the aryl methyl groups, methylene adjacent to the carbonyl, and ethyl groups attached to the tertiary nitrogen. In ^{13}C NMR spectroscopy, the amide carbonyl and differently substituted aromatic carbons occupy distinguishable regions. Chemical shifts, multiplicities, and band positions are dependent on solvent, concentration, temperature, and whether the analyzed material is the free base or a salt (Pavia et al., 2015).

A particularly useful synthesis-related comparison is the disappearance of the chloromethylene environment of the 2-chloroacetamide precursor and the corresponding appearance of the amino-substituted methylene environment in the product.

Specifically, displacement of the electronegative chlorine atom in 2-chloro-N-(2,6-dimethylphenyl)acetamide by the less electronegative diethylamino group produces a characteristic upfield shift of the α-methylene protons from δ 4.16 ppm (–CH_2Cl) to δ 3.14 ppm (–CH_2N–) in ^1H NMR ($CDCl_3$), providing a clear diagnostic spectroscopic marker of reaction progress as detailed in the "Analytical Characterization and Pharmaceutical Quality" section (Perri et al., 2026).

Chemical Synthesis of Lidocaine

Conventional two-step synthesis

A well-established preparation starts from 2,6-dimethylaniline. In the first step, reaction with chloroacetyl chloride produces 2-chloro-N-(2,6-dimethylphenyl)acetamide through nucleophilic acyl substitution. In the second step, diethylamine replaces the chlorine at the α-methylene carbon of the intermediate through an S_N2 pathway, generating lidocaine (Reilly, 1999). The sequence can be summarized as: 2,6-dimethylaniline → 2-chloro-N-(2,6-dimethylphenyl)acetamide → lidocaine.

Reilly (1999) described an instructional laboratory preparation with an overall yield of approximately 71% relative to 2,6-dimethylaniline. This value belongs to the published experimental conditions and should not be generalized to industrial manufacture or unrelated synthetic protocols.

Mechanistic distinction between acylation and S_N2 substitution

In the first transformation, although chloroacetyl chloride possesses two electrophilic carbons—the sp2 acyl carbonyl carbon and the sp3 α-chloromethylene carbon—the nucleophilic nitrogen of 2,6-dimethylaniline attacks exclusively at the far more electrophilic acyl carbonyl center. Formation of a tetrahedral intermediate is followed by carbonyl re-formation and chloride expulsion, yielding

the α-chloroacetamide through chemoselective nucleophilic acyl substitution rather than electrophilic aromatic substitution. In classical laboratory protocols, this reaction is conducted in glacial acetic acid buffered with aqueous sodium acetate; buffering neutralizes the liberated HCl and prevents protonation of 2,6-dimethylaniline into a non-nucleophilic anilinium ion (Carey & Sundberg, 2007; Reilly, 1999).

In the second transformation, diethylamine attacks the primary sp3 carbon of the $–CH_2Cl$ group adjacent to the amide carbonyl in a concerted SN2 process, typically carried out in refluxing toluene. Because the displaced chlorine resides on an aliphatic α-carbon rather than the aromatic ring, classical SN_2 kinetics apply. Excess diethylamine (typically 2.5–3.0 equivalents) is employed so that one equivalent serves as the carbon nucleophile while an additional equivalent acts as a sacrificial Brønsted base to scavenge liberated HCl as insoluble diethylammonium chloride, driving the substitution to completion (Reilly, 1999).

Assessment of alternative synthetic proposals

Alternative routes are scientifically meaningful only when their reagents, intermediates, bond-forming steps, and product identity are consistent. In particular, direct mixing of a carboxylic acid and an aniline should not automatically be described as an efficient amide formation without a suitable activation or coupling strategy. Similarly, esterification, amide formation, and substitution at an α-halo carbon are chemically distinct operations. A proposed route should not be presented as established until primary experimental evidence is available.

More sustainable synthesis and downstream processing

Beyond bond formation, sustainable process design addresses solvent demand, extraction efficiency, reagent stoichiometry, energy consumption, and waste generation. Perri et

al. (2026) developed a fully integrated, one-pot synthesis of lidocaine conducted in a hydrophilic deep eutectic solvent (DES) composed of choline chloride and urea (ChCl:U, 1:2 molar ratio, reline), coupled with direct liquid–liquid extraction into a hydrophobic DES consisting of L-menthol and decanoic acid (1:1 molar ratio). In the first step, the hydrogen-bonding network of ChCl:U, which the authors propose activates chloroacetyl chloride, allowed nucleophilic acyl substitution at 25 °C without added base or catalyst, affording the α-chloro-2,6-dimethylacetanilide intermediate in 92% isolated yield within 20 min (whereas the acidic DES ChCl:lactic acid gave no conversion, most likely because of protonation of the aniline). Without isolating the intermediate, subsequent addition of 1.5 equivalents of diethylamine at 50 °C in the same ChCl:U medium afforded lidocaine in 90% overall isolated yield, while recycling of the hydrophilic DES across three consecutive cycles maintained yields of 90%, 88%, and 77%.

This dual-DES strategy demonstrates that reaction media, work-up extraction, and biocompatible formulation matrices can be engineered as an integrated system without volatile organic compounds (VOCs). Evaluated quantitatively using CHEM21 green chemistry metrics, the DES-mediated process achieved an atom economy (AE) of 76%, a reaction mass efficiency (RME) of 61%, an optimum efficiency (OE) of 80.4%, and a low process mass intensity (PMI) of 6.4 g g−1 (with a solvent intensity PMIsolv of 4.8 g g−1), whereas the conventional and multi-component routes used for comparison show PMI values ranging from 11.9 to 816.2 g g−1 (Perri et al., 2026).

Conversion to pharmaceutically relevant salts

Following isolation, lidocaine free base may be converted into a salt such as lidocaine hydrochloride by protonation of the terminal tertiary amine. Salt formation influences dissolution and

formulation suitability without changing the covalent framework of the lidocaine molecule. Synthetic procedures and analytical reports must specify whether the tested material is the free base, hydrochloride, or another form (National Center for Biotechnology Information, n.d.).

Structure–Activity Relationships and Physicochemical Behavior

The classical structural arrangement of many local anesthetics includes a lipophilic aromatic region, an intermediate linkage, and an ionizable amino terminus. In lidocaine, the aromatic region contributes hydrophobic surface area, the amide linkage influences chemical and metabolic behavior, and the tertiary amine governs a substantial component of the pH-dependent charge distribution. Their effects are interdependent rather than additive in a simple numerical sense (Becker & Reed, 2012; Butterworth & Strichartz, 1990).

Ionization and membrane access

Lidocaine behaves as a weak base whose tertiary diethylamino group exhibits a pKa of approximately 7.9 at 25 °C (~7.7 at 37 °C). The ratio of its uncharged free base (B) to protonated cationic form (BH+) is governed by the Henderson–Hasselbalch relation: pH = pKa + log([B]/[BH+]). At physiological pH (7.4), using pKa 7.9 as an illustrative value, the ratio [B]/[BH+] equals 10^(7.4−7.9) ≈ 0.316, meaning that roughly one quarter (about 24%) of lidocaine exists as the neutral lipid-soluble base (B) capable of diffusing across the axonal membrane, while about 76% exists as the protonated cation (BH+) that binds to the intracellular vestibule of the sodium channel. Using the lower pKa of ~7.7 expected at 37 °C, the uncharged fraction would be closer to one third. Classical electrophysiological studies demonstrated that while the cationic species is the predominant active blocker at the inner pore,

uncharged molecules can also access the channel via hydrophobic membrane pathways (Hille, 1977; Strichartz, 1981).

This relatively large uncharged fraction at pH 7.4 contributes to the rapid clinical onset of lidocaine (typically 2–5 min) compared with local anesthetics of higher pKa, such as bupivacaine (pKa 8.1; ~17% free base) or procaine (pKa 8.9; ~3% free base). Conversely, in inflamed or infected tissues where localized lactic acidosis lowers extracellular pH to 6.0–6.5, the uncharged fraction of lidocaine falls to roughly 1.2–3.8%, leaving most of the drug in its poorly membrane-permeant BH+ form and thereby reducing the amount that can reach the axonal membrane, which, together with faster vascular washout in hyperemic inflamed tissue, can attenuate anesthetic efficacy (Becker & Reed, 2012).

Lipophilicity, protein binding, and amide stability

Greater lipophilicity may promote membrane affinity, but it can simultaneously influence tissue distribution, nonspecific binding, and systemic exposure. Plasma protein binding affects the free circulating fraction, while hepatic biotransformation is an important determinant of systemic lidocaine disposition. The resonance-stabilized amide differs chemically from ester linkages; nevertheless, amide character does not make the drug non-toxic, nor does aromatic substitution alone determine the pharmacological profile (Becker & Reed, 2012).

Changes to the aromatic substituents can modify steric dimensions and hydrophobicity, whereas changes near the amino nitrogen may alter pK_a and solubility. Any structure–activity hypothesis must therefore be evaluated against target-channel binding, ionization, access pathways, and distribution instead of resting on a single electronic effect (Butterworth & Strichartz, 1990; O'Leary & Chahine, 2018).

Pharmacological Mechanism of Action

Lidocaine reduces sodium influx through voltage-gated sodium channels and thereby inhibits the generation and conduction of propagated electrical impulses in peripheral nerve fibers. Sodium channels cycle among resting, open, and inactivated conformations; the apparent block can depend on the channel state and the frequency of repeated stimulation. State-dependent and use-dependent effects provide a more accurate description than the simplistic notion of a permanent closure of the channel pore (Hille, 1977; O'Leary & Chahine, 2018).

At the molecular level, the pore-forming α-subunit of voltage-gated sodium channels comprises four homologous domains (DI–DIV), each containing six transmembrane segments (S1–S6). Lidocaine binds within the inner aqueous pore lined by the S6 helices, interacting specifically with conserved aromatic residues on Domain IV Segment 6 (DIV-S6)—most notably Phenylalanine-1760 (Phe1760) and Tyrosine-1767 (Tyr1767) in cardiac Nav1.5 channels and their homologous counterparts in the skeletal-muscle Nav1.4 isoform and the neuronal Nav1.7 and Nav1.8 isoforms. Within this binding site, the 2,6-dimethylphenyl ring is thought to engage in hydrophobic and aromatic π–π stacking interactions, while the protonated diethylammonium group (BH+) is thought to form a cation–π interaction with Phe1760. In ventricular myocardium, rapid binding and rapid unbinding from inactivated Nav1.5 channels during diastole explain lidocaine's Vaughan Williams class Ib antiarrhythmic profile, which requires carefully monitored intravenous dosing distinct from local infiltration (O'Leary & Chahine, 2018).

Pharmacokinetics, Pharmaceutical Forms, and Clinical Scope

Systemic absorption depends on the administration site, local blood flow, administered amount, pharmaceutical formulation, and

the presence or absence of a vasoconstrictor. In certain preparations, epinephrine may reduce local vascular uptake, which can prolong regional action and modify systemic exposure. Such effects must not be generalized to every anatomical site or patient. Protein binding and hepatic metabolism further influence systemic drug concentrations (Becker & Reed, 2012).

Following systemic absorption, lidocaine undergoes extensive hepatic first-pass metabolism (~70% hepatic extraction ratio), limiting its oral bioavailability to approximately 35% and precluding oral antiarrhythmic administration. Hepatic biotransformation proceeds primarily via cytochrome P450-mediated oxidative N-dealkylation catalyzed by CYP1A2 and CYP3A4, sequentially removing the ethyl groups to yield the active metabolite monoethylglycinexylidide (MEGX)—which retains significant sodium-channel blocking and convulsant activity—followed by glycinexylidide (GX). Subsequent cleavage of the carboxamide linkage by hepatic microsomal amidases/carboxylesterases generates 2,6-xylidine (2,6-dimethylaniline), which is further hydroxylated at the para position to 4-hydroxy-2,6-xylidine, the major urinary metabolite accounting for roughly 70% of the excreted dose. Unlike ester-type local anesthetics (e.g., procaine), which are hydrolyzed by plasma pseudocholinesterase to release allergenic para-aminobenzoic acid (PABA), amide-linked lidocaine does not form PABA, making true IgE-mediated allergic reactions exceedingly rare (Becker & Reed, 2012).

Lidocaine is supplied in formulations appropriate for injection or topical administration, including solutions, gels, creams, and sprays; selected medicated patches are used for specific pain conditions. The authorization of a particular product and its indications depend on jurisdiction and should be checked against the corresponding prescribing information. Dental anesthesia, minor

procedures, nerve blocks, superficial interventions, topical symptom control, and selected cardiac indications represent different clinical contexts rather than interchangeable methods of administration (Gudin & Nalamachu, 2020).

A distinction must also be maintained among an established pharmacological effect, an authorized product indication, and an investigational application. Beyond classical axonal sodium-channel blockade, systemic intravenous lidocaine modulates N-methyl-D-aspartate (NMDA) receptors, glycine receptors, G-protein-coupled pathways, and polymorphonuclear granulocyte priming, which underlie its perioperative antihyperalgesic and anti-inflammatory properties. Nevertheless, lidocaine should not be characterized broadly as a routine sedative, nor should a single preparation be assumed suitable for all ophthalmic or specialized clinical uses (Hermanns et al., 2019).

Toxicity and Safety

At sufficiently high systemic exposures, local anesthetics can cause serious central nervous system and cardiovascular effects. Circumoral numbness, metallic taste, tinnitus, dizziness, and agitation may occur, while severe cases can include seizures, impaired consciousness, conduction abnormalities, and cardiovascular collapse. Presentation is variable, and not all patients exhibit a stereotypical progression of symptoms (El-Boghdadly et al., 2018; Gitman et al., 2019).

Local anesthetic systemic toxicity (LAST) is not restricted to straightforward dose excess. Accidental intravascular injection, rapid absorption from a highly perfused site, cumulative exposure, and patient-specific vulnerabilities may contribute. Prevention, early recognition, and immediate airway and circulatory management are therefore central; in severe cardiovascular or neurological LAST, 20% intravenous lipid emulsion (ILE) therapy is thought to act as a

'lipid sink' (or 'lipid shuttle') that partitions lipophilic anesthetic molecules away from cardiac and cerebral tissues toward hepatic metabolic clearance while also supporting myocardial fatty-acid metabolism, although the exact mechanisms are still under investigation (El-Boghdadly et al., 2018; Gitman et al., 2019).

The aromatic ring should not be identified as the sole or direct cause of systemic toxicity. Molecular structure shapes tissue partitioning and pharmacodynamics, but clinical risk is determined jointly by exposure, administration conditions, physiology, and the drug's disposition. Mechanistic structure–activity analyses and clinical safety assessments are complementary, not interchangeable.

Analytical Characterization and Pharmaceutical Quality

A synthetic product cannot be identified conclusively by color, melting point, or thin-layer chromatography alone. IR and NMR spectra offer complementary structural evidence, appropriate mass spectrometric data support molecular composition, and chromatographic methods provide information on components and impurities. A defensible analytical report should distinguish the chlorinated intermediate from lidocaine and specify the measured chemical form and experimental conditions.

The analytical characterization reported by Perri et al. (2026) in $CDCl_3$ (500 MHz for ^{1}H, 125 MHz for ^{13}C) illustrates the main spectral features of lidocaine and its distinction from the α-chloro-2,6-dimethylacetanilide precursor. Whereas the chlorinated intermediate exhibits a deshielded $–CH_2Cl$ singlet at δ 4.16 ppm (13C: δ 42.7 ppm) and an amide N–H signal at δ 7.38 ppm, conversion to lidocaine shifts the α-methylene ($–CH_2N–$) singlet upfield to δ 3.14 ppm (2H; 13C: δ 57.7 ppm) and shifts the amide N–H proton downfield to δ 8.84 ppm (br s, 1H) due to intramolecular hydrogen bonding with the tertiary amine nitrogen. The remaining 1H NMR resonances of lidocaine appear at δ 7.01–6.99 ppm (m, 3H,

Ar–H), δ 2.63–2.59 ppm (q, 4H, N(CH_2CH_3)2; 13C: δ 49.1 ppm), δ 2.15 ppm (s, 6H, two Ar–CH_3; 13C: δ 18.7 ppm), and δ 1.06 ppm (t, 6H, N(CH_2CH_3)2; 13C: δ 12.8 ppm), alongside the amide carbonyl 13C signal at δ 170.4 ppm. Diagnostic FT-IR absorptions include the amide N–H stretch at 3245 cm−1, aliphatic C–H stretches at 2967 and 2799 cm−1, the sharp Amide I (C=O) band at 1661 cm−1, the Amide II / aromatic skeletal band at 1490 cm−1, and the characteristic out-of-plane C–H bending vibration of the 1,2,3-trisubstituted benzene ring at 763 cm−1. In electron-impact mass spectrometry (EI-MS, 70 eV), α-cleavage yields the diagnostic base peak at m/z 86 (100%, [CH2=N(C2H5)2]+) together with the molecular ion at m/z 234 (M+•, 7%), while positive-mode HR-ESI-MS confirms the protonated molecular ion [M+H]+ at m/z 235.1800 (calculated: 235.1810) (Perri et al., 2026).

Signal assignment must account for integration, multiplicity, molecular symmetry, and chemical-shift variations induced by solvent, temperature, and hydrochloride salt formation. Because accurate mass measurement confirms elemental composition rather than bulk purity, pharmacopoeial quality control (e.g., European Pharmacopoeia and United States Pharmacopeia monographs) mandates liquid chromatographic quantification of synthesis- and degradation-related impurities. Two impurities are of particular concern: 2,6-dimethylaniline (2,6-xylidine; Impurity A), which serves as both the synthetic precursor and a possible hydrolytic degradation product, and the electrophilic, alkylating intermediate 2-chloro-N-(2,6-dimethylphenyl)acetamide, which must also be controlled as a process-related impurity. Because 2,6-dimethylaniline is classified by IARC as possibly carcinogenic to humans (Group 2B), pharmacopoeial monographs enforce strict limits (the current monograph should be consulted for exact values) alongside dosage-form-specific controls for sterility, endotoxins, pH, and assay potency.

Conclusions

Lidocaine demonstrates how one pharmaceutical molecule can connect the electronic principles of aromaticity to synthetic reactivity, physicochemical behavior, and drug action. Its 2,6-dimethylphenyl moiety provides an aromatic, lipophilic component whose steric environment must be interpreted together with the resonance-stabilized amide and protonatable tertiary amino group. The conventional synthesis also offers a clear teaching example of the difference between nucleophilic acyl substitution and S_N2 substitution at a primary alkyl carbon.

Its therapeutic action is not reducible to a single functional group: membrane access, charge state, channel conformation, metabolism, and clinical context jointly determine behavior. Current process research illustrates how conventional bond-forming chemistry can be integrated with redesigned solvent and recovery strategies. Finally, properly sourced spectroscopic characterization and carefully qualified safety statements are indispensable to translating an organic-chemical description into a rigorous pharmaceutical account.

References

Becker, D. E., & Reed, K. L. (2012). Local anesthetics: Review of pharmacological considerations. *Anesthesia Progress*, *59*(2), 90–101. https://doi.org/10.2344/0003-3006-59.2.90

Butterworth, J. F., IV, & Strichartz, G. R. (1990). Molecular mechanisms of local anesthesia: A review. *Anesthesiology*, *72*(4), 711–734. https://doi.org/10.1097/00000542-199004000-00022

Carey, F. A., & Sundberg, R. J. (2007). *Advanced organic chemistry: Part A: Structure and mechanisms* (5th ed.). Springer.

El-Boghdadly, K., Pawa, A., & Chin, K. J. (2018). Local anesthetic systemic toxicity: Current perspectives. *Local and Regional Anesthesia*, *11*, 35–44. https://doi.org/10.2147/LRA.S154512

Gitman, M., Fettiplace, M. R., Weinberg, G. L., Neal, J. M., & Barrington, M. J. (2019). Local anesthetic systemic toxicity: A narrative literature review and clinical update on prevention, diagnosis, and management. *Plastic and Reconstructive Surgery*, *144*(3), 783–795. https://doi.org/10.1097/PRS.0000000000005989

Gudin, J., & Nalamachu, S. (2020). Utility of lidocaine as a topical analgesic and improvements in patch delivery systems. *Postgraduate Medicine*, *132*(1), 28–36.

Hermanns, H., Hollmann, M. W., Stevens, M. F., Lirk, P., Brandenburger, T., Piegeler, T., & Werdehausen, R. (2019). Molecular mechanisms of action of systemic lidocaine in acute and chronic pain: a narrative review. *British Journal of Anaesthesia*, *123*(3), 335–349. https://doi.org/10.1016/j.bja.2019.06.014

Hille, B. (1977). Local anesthetics: Hydrophilic and hydrophobic pathways for the drug–receptor reaction. *The Journal of General Physiology*, *69*(4), 497–515. https://doi.org/10.1085/jgp.69.4.497

National Center for Biotechnology Information. (n.d.). *PubChem compound summary for lidocaine*. PubChem. Retrieved October 24, 2026, from https://pubchem.ncbi.nlm.nih.gov/compound/Lidocaine

O'Leary, M. E., & Chahine, M. (2018). Mechanisms of drug binding to voltage-gated sodium channels. In M. Chahine (Ed.), *Voltage-gated sodium channels: Structure, function and channelopathies* (pp. 209–231). Springer. https://doi.org/10.1007/164_2017_73

Pavia, D. L., Lampman, G. M., Kriz, G. S., & Vyvyan, J. R. (2015). *Introduction to spectroscopy* (5th ed.). Cengage Learning.

Perri, A., Parrotta, L. C., Gencarelli, S., Sole, R., Dragostin, O. M., Guillena, G., & Di Gioia, M. L. (2026). Integrating green synthesis and liquid–liquid extraction of lidocaine in deep eutectic solvents. *RSC Medicinal Chemistry*, *17*, 1474–1482. https://doi.org/10.1039/D5MD00922G

Reilly, T. J. (1999). The preparation of lidocaine. *Journal of Chemical Education*, *76*(11), 1557. https://doi.org/10.1021/ed076p1557

Smith, M. B., & March, J. (2007). *March's advanced organic chemistry: Reactions, mechanisms, and structure* (6th ed.). Wiley-Interscience.

Strichartz, G. R. (1981). Current concepts of the mechanism of action of local anesthetics. *Journal of Dental Research*,

60(8), 1460–1467. https://doi.org/10.1177/0022034581060008090 4

BÖLÜM 3

UTILIZATION OF ESSENTIAL OILS IN POLYMERIC FOOD PACKAGING

ZEHRA KURU[1],
MEHMET ARİF KAYA[2]

Introduction

Essential oils (EOs) are concentrated, hydrophobic, volatile secondary metabolites synthesized by aromatic and medicinal plants. Biosynthesized in specialized secretory structures—including glandular trichomes, secretory cavities, resin canals, and epidermal cells—EOs function in planta primarily as defensive biochemical barriers against phytopathogenic microorganisms, herbivores, and environmental stressors, while also serving as chemical attractants for pollinators (Bakkali et al., 2008).

Chemically, essential oils are complex, multicomponent mixtures comprising tens to hundreds of individual volatile organic compounds (VOCs) at varying concentrations (Dhifi et al., 2016). These

[1] PhD Student, Yalova University, Institute of Graduate Studies, Department of Polymer Materials Engineering, ORCID: 0000-0002-1920-4412
[2] Assoc. Prof. Dr., Yalova University, Faculty of Engineering, Department of Polymer Materials Engineering, ORCID: 0000-0001-9339-3381

constituents predominantly belong to two distinct biosynthetic pathways.

Terpenoids and terpenes form via the mevalonic acid or methylerythritol phosphate (MEP) pathways. This group encompasses monoterpene hydrocarbons (e.g., limonene, pinene, p-cymene), oxygenated monoterpenes (e.g., thymol, carvacrol, linalool, menthol, 1,8-cineole), sesquiterpenes (e.g., β-caryophyllene), and their oxygenated derivatives.

Phenylpropanoids are synthesized through the shikimic acid pathway, yielding aromatic compounds characterized by a three-carbon side chain attached to a benzene ring (e.g., eugenol, cinnamaldehyde, anethole, vanillin (Dhifi et al., 2016).

The biological efficacy of an essential oil is typically governed by its major active compounds (often constituting 20% to 85% of the total blend), although synergistic, additive, or antagonistic interactions with minor constituents frequently dictate the overall antimicrobial and antioxidant spectrum (Burt, 2004; Dhifi et al., 2016).

Historical Evolution of EOs

The ancient Egyptians documented the use of aromatic resins and plant extracts in mummification, perfumery, and medical formulations as early as 3000 BCE, recorded in documents such as the Ebers Papyrus. Concurrently, ancient Indian Ayurvedic traditions and Traditional Chinese Medicine incorporated aromatic botanical distillates for therapeutic and preservative purposes (Sadgrove & Jones, 2015; Sharifi-Rad et al., 2017).

Although primitive extraction relied on maceration and lipid infusion, distillation technology was substantially refined between the 9th and 11th centuries CE in the Islamic Golden Age, and the

physician and polymath Ibn Sina (Avicenna) is widely credited with improving condensation through a cooling coil, an innovation associated with the production of rose oil and hydrosols from Rosa damascene.

During the 16th and 17th centuries, essential oils entered European pharmacopeias ("quinta essentia"). The 19th and 20th centuries established modern analytical characterization through gas chromatography coupled with mass spectrometry (GC-MS), facilitating molecular-level chemical isolation, quality standardization, and commercial industrialization across the food, fragrance, and pharmaceutical sectors (Sadgrove & Jones, 2015).

Industrial and Functional Applications of EOs

Essential oils have applications across several industries, where their distinctive aromas are valued alongside their biological properties. Their suitability for a particular product depends on the oil's composition, concentration, and intended function. Regulatory acceptance is also specific to the substance and its use. In the United States, certain essential oils and natural extractives are generally recognized as safe (GRAS) under their intended conditions of food use. In the European Union, EFSA provides scientific safety assessments that support the European Commission's authorization decisions for relevant food flavorings. These frameworks should therefore be considered in relation to the particular oil and application.

One of the most familiar uses of essential oils is to shape the sensory character of everyday products. In foods and beverages, they contribute characteristic flavors and aromas, while in cosmetics and fine perfumery they help create recognizable scent profiles. Their aromatic complexity allows formulators to introduce fresh, floral, herbal, or spicy notes and adjust how these notes interact with other ingredients. Selecting a suitable oil involves considering its

compatibility with the formulation, its stability during processing and storage, and the consistency of its sensory properties (Atarés & Chiralt, 2016).

Beyond their sensory contribution, selected essential oils have attracted research interest for their antimicrobial, anti-inflammatory, and analgesic potential. For example, experimental studies have reported anti-inflammatory and antinociceptive effects of rosemary essential oil in animal models, illustrating one direction of investigation without establishing equivalent clinical effects in humans (Bakkali et al., 2008).

In topical and personal care formulations, the practical challenge is to combine the desired activity with suitable stability and skin compatibility. Concentration, purity, and formulation therefore require careful attention, since plant origin alone does not establish the safety of a finished product.

Essential oils are also being investigated as ingredients in botanical pest-control products and postharvest antifungal treatments. Experimental research has examined their insecticidal activity against agricultural pests, including aphids, as well as their potential to limit fungal decay in harvested produce. Their volatility enables fumigation treatments, in which active constituents are delivered through the atmosphere surrounding stored commodities. Such approaches may help reduce reliance on selected conventional treatments, although their performance depends on the target organism, exposure conditions, and compatibility with the crop. Research on fruit storage also shows why treatments must be evaluated against the specific pathogens present: an oil treatment that suppresses one fungal disease may favor another (Atarés & Chiralt, 2016).

In perishable foods—including meat, seafood, dairy products, bakery products, and fresh fruits—essential oils are being explored as

ingredients to slow microbial deterioration and oxidative quality losses (Burt, 2004). Their antioxidant contribution can help delay lipid oxidation, as demonstrated in research on oregano essential oil in chicken meat (Petrou et al., 2012; Zheng et al., 2023). They may be added directly to a food or incorporated into edible coatings and active packaging films. Studies of oil-containing films illustrate how these systems can combine antimicrobial and antioxidant functions to support product preservation (Ribeiro-Santos et al., 2017). Successful formulation requires balancing preservation and sensory acceptance: the oil must provide useful activity while remaining compatible with the food's characteristic taste and aroma (Atarés & Chiralt, 2016).

Critical Performance Metrics for Food Packaging Materials

Food packaging must protect a product throughout processing, storage, transportation, and retail display. Maintaining this protection requires a combination of barrier properties, mechanical reliability, thermal stability, effective sealing, and chemical safety. The appropriate specification depends on the food's composition, its sensitivity to environmental conditions, and its intended shelf life. A package designed for crisp, moisture-sensitive foods, for example, faces different demands from one intended for fresh produce that continues to respire after harvest.

The water vapor transmission rate (WVTR) describes how readily water vapor passes through a packaging material under specified conditions, commonly expressed in g m^{-2} day^{-1}. Controlling this transfer helps preserve the moisture balance responsible for a food's characteristic texture and appearance. Dry products, such as crackers and breakfast cereals, need protection against moisture uptake and the resulting loss of crispness. Fresh products require moisture management that limits dehydration while accounting for possible condensation within the package. WVTR measurements should

therefore be interpreted alongside the test temperature, relative humidity, and material thickness, with comparisons made under consistent conditions.

The oxygen transmission rate (OTR) indicates the rate at which oxygen passes through a material under defined test conditions. Restricting oxygen ingress can help delay oxidative deterioration and limit the growth of aerobic spoilage microorganisms. The required barrier must still match the product. Fresh fruits and vegetables continue to consume oxygen after harvest, so their packaging must provide gas exchange compatible with their respiration rate. Research on fresh-cut lettuce demonstrates that an unsuitable combination of film OTR and initial oxygen concentration can create anaerobic conditions and promote undesirable fermentation odors. Microbiological safety also requires consideration of hazards associated with reduced-oxygen environments, particularly for susceptible foods.

Light transmission becomes particularly important when a food contains photosensitive nutrients, pigments, or compounds that initiate oxidation. Packaging that attenuates relevant ultraviolet and visible wavelengths can help limit lipid photo-oxidation, nutrient degradation, discoloration, and the development of undesirable flavors. Effective protection depends on the wavelengths transmitted as well as the total amount of light reaching the food. Studies of milk packaging, for example, show that visible wavelengths can contribute to photo-oxidation and that protection must account for the absorption characteristics of photosensitizers such as riboflavin. Light-barrier performance should consequently be evaluated against the product's sensitivity and its expected display conditions.

Packaging experiences stretching, bending, compression, vibration, and contact with sharp edges during filling and distribution. Its mechanical properties must provide sufficient protection under

these conditions. A rigid container needs dimensional stability, whereas a flexible pouch may require greater extensibility and toughness. Puncture and tear resistance provide additional information about resistance to localized damage. Test conditions, specimen dimensions, and loading rate must be controlled when comparing materials, since they can substantially influence the measured results.

Packaging must retain the properties required for its intended processing and storage conditions. For polymer-based materials, relevant measurements include the glass transition temperature (Tg), the melting temperature (Tm) of crystalline regions where present, and the onset of thermal degradation (Td_{onset}). These measurements help explain changes in stiffness, flexibility, dimensional stability, and processability with temperature. The measured thermal profile must be interpreted in relation to the actual application, including chilled storage, freezing, hot filling, or thermal processing.

Reliable closure is essential for maintaining the protection provided by the packaging structure. A suitable heat-sealing window allows consistent seals to form across a practical range of sealing temperatures, pressures, and contact times. The resulting closure must withstand handling and distribution while providing the opening characteristics required by the consumer. Laboratory seal-strength measurements help characterize this performance and support process development. Finished-package evaluation should also address seal continuity and leakage, since a material with favorable barrier properties can still provide inadequate protection when its closure contains channels or other defects (Robertson, 2016).

Food-contact packaging must be sufficiently compatible with its contents to protect human health and preserve acceptable food composition, taste, and odor. This requires attention to substances that may transfer from the packaging into food, including relevant

constituents of polymers, coatings, adhesives, and printing systems. The governing principle is that such transfer must remain within applicable safety requirements and must avoid unacceptable changes in the food's sensory properties (Atarés & Chiralt, 2016).

Overall migration limits (OMLs) and specific migration limits (SMLs) address complementary aspects of this assessment. Overall migration testing evaluates aggregate transfer under prescribed conditions, while specific migration limits control the transfer of particular substances. Compliance testing must reflect the intended food type, contact duration, and temperature, using appropriate foods or food simulants. Active packaging systems that intentionally release functional substances require additional consideration under the rules governing their intended activity (Ribeiro-Santos et al., 2017).

Historical Evolution of Packaging Substrates

The development of food packaging has closely followed changes in how people produce, store, transport, and consume food. Early containers addressed immediate needs, such as carrying harvested crops or protecting food during short journeys. As trade expanded and food distribution grew more complex, packaging took on additional functions, including extending shelf life, maintaining product quality, and supporting large-scale manufacturing. Over time, these developments created a diverse range of materials that continue to coexist in modern packaging systems (Ribeiro-Santos et al., 2017).

The earliest forms of packaging relied on materials available in the surrounding environment. Leaves, animal skins, gourds, woven plant fibers, and carved wood could be adapted into wrappers, baskets, bags, and vessels. Their use reflected local resources, food practices, and practical craftsmanship. A gourd could hold liquids, while woven fibers provided a convenient way to carry harvested produce. Although these materials offered useful physical protection, their

performance varied with their structure, preparation, and exposure to moisture. They established the basic relationship between a food product, its container, and the conditions under which it was stored or transported.

Ceramic pottery expanded food storage by providing rigid vessels that could be shaped for different purposes. Glassmaking later introduced another important container material. Archaeological research documents glass-vessel production in Mesopotamia and Egypt around the middle of the second millennium BCE, establishing manufacturing traditions that would eventually support much wider uses of glass containers.

Paper developed through a different technological pathway. Its origins in China predate the improvements traditionally associated with Cai Lun in 105 CE during the Eastern Han dynasty. Refining papermaking helped establish a versatile sheet material that could later be adapted for wrapping, labeling, and, with later manufacturing developments, paperboard packaging. Paper's flexibility and suitability for printing eventually made it valuable for both protecting products and communicating information about them.

The early nineteenth century brought a closer connection between packaging design and heat preservation. In 1810, Peter Durand patented a method for preserving food in sealed containers, including vessels made from tin-plated iron. This was an important step toward commercial canning, which combined a protective container with a preservation process. An early food-preservation can made by Bryan Donkin and Company in 1812 shows how quickly this approach moved into practical manufacture.

During the twentieth century, advances in polymer chemistry and industrial processing greatly broadened the materials available to packaging manufacturers. Developments in polyethylene and

polypropylene production were particularly significant, helping establish polymers that could be manufactured in large quantities and shaped into many useful forms. Established food-packaging materials included low-density polyethylene (LDPE), high-density polyethylene (HDPE), polypropylene (PP), polyethylene terephthalate (PET), polystyrene (PS), polyvinyl chloride (PVC), and ethylene vinyl alcohol copolymer (EVOH).

Their industrial appeal came from a combination of low weight, production efficiency, versatility, and a wide range of mechanical and barrier properties. Manufacturers could select materials for flexible films, rigid containers, bottles, trays, or protective foams, and combine different polymers in layered structures. EVOH, for example, became valuable as a gas-barrier component in food packaging. This ability to assign different functions to individual layers enabled packaging to be tailored more closely to the needs of particular foods (Robertson, 2016).

The widespread use of conventional plastics also created concerns about resource consumption, waste management, and environmental persistence. Plastics that escape collection systems can accumulate on land and in aquatic environments, while fragmentation can generate smaller particles, including microplastics. These concerns have encouraged research into renewable feedstocks, alternative polymers, and packaging systems compatible with improved waste-management practices (Siracusa et al., 2008).

Economic Dimensions and Market Dynamics

The global food packaging market was valued at approximately USD 421.6 billion in 2025 and is projected to reach USD 599.0 billion by 2033, corresponding to a compound annual growth rate (CAGR) of 4.3% (Grand View Research, 2026). Flexible packaging formats (pouches, barrier films, shrink wraps) constitute the largest segment,

accounting for more than 44% of revenue in 2025, and are also among the fastest-growing (Grand View Research, 2026).

Global initiatives addressing food loss and waste, where an estimated one-third of all food produced for human consumption—about 1.3 billion tonnes per year—is lost or wasted across the food supply chain, from agricultural production to final household consumption (Gustavsson et al., 2011).

Stringent international packaging waste regulations—most notably Regulation (EU) 2025/40 on packaging and packaging waste (PPWR), which replaced Directive 94/62/EC and applies from 12 August 2026—establish mandatory requirements for recyclability, recycled content, reuse formats, and waste prevention, thereby favouring lightweight, material-efficient and recyclable active packaging designs (European Commission, 2026).

Rationales and Roles of Essential Oils in Polymeric Food Packaging

Conventional passive packaging acts solely as an inert physical barrier that protects food from external environmental factors. In contrast, active food packaging deliberately incorporates active components intended to release substances into the packaged food or its headspace, or absorb substances from the food environment, to preserve freshness, safety, and extend shelf life (Dainelli et al., 2008).

Incorporating essential oils into polymeric packaging films shifts the food preservation approach from direct bulk food dosing to controlled interface release.

Adding free EOs directly to food formulations frequently produces strong, undesirable organoleptic profiles (herbaceous, pungent, or medicinal off-flavors) and risks early volatilization or chemical binding with food lipids/proteins (Atarés & Chiralt, 2016).

Microbial colonization and oxidative spoilage predominantly initiate at the food surface. Polymeric carriers act as sustained-release reservoirs, maintaining a continuous minimum inhibitory concentration (MIC) in the food headspace and surface microenvironment throughout storage (Burt, 2004).

Antimicrobial Mechanisms of Action

The antimicrobial spectrum of EOs covers foodborne Gram-positive and Gram-negative bacteria, molds, and yeasts. Because of their multicomponent lipophilic chemistry, EOs act simultaneously upon several cellular targets, avoiding the rapid emergence of microbial resistance (Nazzaro et al., 2013).

Lipophilic monoterpenes partition directly into the phospholipid bilayer of bacterial membranes. This destabilizes the membrane structure, increases fluidity, and forms non-specific hydrophilic pores (Bakkali et al., 2008; Nazzaro et al., 2013).

Phenolic hydroxyl moieties (as in thymol, carvacrol, and eugenol) act as transmembrane proton carriers. They dissipate the transmembrane electrical potential ($\Delta\Psi$) and pH gradient (ΔpH), uncoupling oxidative phosphorylation and draining intracellular ATP reserves.

Loss of selective membrane permeability causes the rapid efflux of vital intracellular ions (K^+, Mg^{2+}, Ca^{2+}), amino acids, and nucleic acids, ultimately causing irreversible cellular collapse and lysis (Lambert et al., 2001).

Intracellular accumulation of lipophilic compounds inhibits critical metabolic enzymes (e.g., ATPases) and disrupts normal DNA replication and transcription (Bakkali et al., 2008).

Gram-positive bacteria (e.g., Listeria monocytogenes, Staphylococcus aureus) are generally more susceptible to EO actions

than Gram-negative bacteria (e.g., Escherichia coli, Salmonella enterica). Gram-negative bacteria possess an external lipopolysaccharide (LPS) outer membrane that acts as a hydrophilic permeability barrier restricting hydrophobic hydrocarbon influx (Burt, 2004; Nazzaro et al., 2013).

Antioxidant Mechanisms of Action

Lipid auto-oxidation is a major non-microbial pathway driving quality loss, rancidity, toxic aldehyde generation, and nutritional degradation in fat-rich foods. Essential oils rich in phenolic compounds interrupt this oxidative cascade through several concurrent mechanisms (Dhifi et al., 2016).

Phenolic terpenoids act as chain-breaking electron or hydrogen atom donors to lipid peroxyl (LOO·) and alkoxyl (LO·) radicals:

$$ArOH + LOO\cdot \longrightarrow ArO\cdot + LOOH$$

The generated phenoxy radical (ArO·) is stabilized via resonance delocalization across the aromatic ring, terminating radical propagation (Bakkali et al., 2008).

Depending on solvent polarity and substrate structure, compounds like eugenol, carvacrol, and thymol quench reactive oxygen species through HAT or SET pathways.

Certain secondary constituents sequester transition metal ions (Fe^{2+}, Cu^{2+}), inhibiting Fenton-type chemistry and the homolytic decomposition of hydroperoxides (Dhifi et al., 2016).

Senescence Delay and Respiration Modulation in Fresh Produce

Applied to post-harvest fresh fruits and vegetables, EO-functionalized films modify metabolic respiration rates, downregulate ethylene biosynthesis, and inhibit post-harvest fungal pathogens (e.g., Botrytis cinerea, Penicillium expansum, Aspergillus niger), reducing

decay rates while preserving tissue firmness and sensory freshness (Atarés & Chiralt, 2016).

Incorporation Methods of Essential Oils into Polymeric Packaging

Integrating volatile, hydrophobic, and thermally labile plant extracts into solid macromolecular networks presents major chemical and engineering challenges, including high-temperature evaporation, phase separation, polymer plasticization, and rapid, uncontrolled release. To resolve these challenges, several processing techniques have been developed (Atarés & Chiralt, 2016).

Solution Casting (Solvent Casting)

Primarily employed at laboratory and pilot scales for biopolymer matrices (e.g., chitosan, starch, gelatin, cellulose ethers) (Siracusa et al., 2008).

The hydrophilic or polar polymer is dissolved in an appropriate solvent (e.g., aqueous acetic acid for chitosan, hot water for starch/gelatin). Essential oils, often pre-blended with non-ionic surfactants (e.g., Tween 20 or Tween 80) to aid dispersion, are added to the polymer dope. The mixture is homogenized using high-shear mixing or probe ultrasonication to create a stable oil-in-water (O/W) emulsion, cast onto non-stick teflon/acrylic plates, and dried under controlled temperature and relative humidity (20–40 °C; 40–50% RH).

Avoids high thermal exposure, minimizing volatile compound degradation; produces transparent, uniform, defect-free testing films.

High processing times, significant solvent consumption, drying economics, and fundamental limitations in scaling to continuous high-speed industrial lines (Wang et al., 2021).

Melt Processing (Extrusion, Compounding, and Blown Film)

The predominant manufacturing technology for standard thermoplastic packaging materials (LDPE, PP, PLA, PBAT).

Polymer pellets and liquid essential oils (or solid active compounds such as thymol/carvacrol crystals) are fed into a single- or twin-screw extruder. The mixture undergoes thermal melting, mechanical shearing, and interspersing before being pushed through a flat cast-film die or circular blown-film die.

Extrusion temperatures (140–210 °C) often exceed the flashpoints and boiling ranges of lighter monoterpenes, causing volatilization losses that can exceed 50% to 70% (Ramos et al., 2012).

To address this, several approaches can be employed: using twin-screw extruders equipped with downstream liquid injection ports located near the die; maintaining low-temperature profiles in the earlier barrel zones; utilizing concentrated polymer masterbatches; or encapsulating the EO (essential oil/active agent) compounds within thermally stable inorganic or supramolecular carriers prior to extrusion (Atarés & Chiralt, 2016).

Surface Coating, Lamination, and Gravure Printing

Instead of dispersing the active compound throughout the bulk polymer, EOs are formulated into a surface coating lacquer and applied directly to pre-formed base films (e.g., PET, oriented PP, or paperboard).

Roll coating, flexographic/gravure printing, bar coating, or spray deposition applies a thin active matrix layer (typically based on chitosan, polyacrylates, or polyurethane dispersions).

Focuses active agents directly at the package-food interface; reduces the quantity of EO required; avoids exposing the structural

base film to high thermal degradation conditions during primary polymer synthesis (Ribeiro-Santos et al., 2017).

Electrospinning and Electrospraying

A continuous, non-thermal nanotechnology method utilizing high-voltage electrostatic fields (typically 10–30 kV) to draw charged viscoelastic polymer solutions into continuous submicron or nanoscale fibers.

As the electrified jet travels toward a grounded collector, the solvent evaporates rapidly (within milliseconds), entraining EO droplets inside ultrafine polymeric fibers without heat exposure.

Produces active, microporous, high-surface-area mats or functional inner liners for multilayer packaging pouches (Wen et al., 2016).

Advanced Pre-Encapsulation Methodologies

To stabilize EOs against oxidation, minimize volatilization during polymer processing, and tailor sustained release kinetics, pre-encapsulation techniques are increasingly integrated into film formulation.

Nanoemulsions and microemulsions are formulated using high-pressure homogenizers, microfluidizers, or ultrasonic cavitation, reducing EO droplet diameters below 100 nm. Sub-micron droplet sizes reduce gravitational phase separation and creaming, improve optical transparency, and enhance interfacial contact with bacterial cells (Donsì & Ferrari, 2016).

β-Cyclodextrin is a cyclic oligosaccharide comprising seven glucopyranose units forming a truncated cone with a hydrophilic exterior and a hydrophobic central cavity. Lipophilic volatile molecules (e.g., cinnamaldehyde, carvacrol, thymol) spontaneously

form non-covalent host-guest inclusion complexes. This supramolecular configuration raises the thermal degradation threshold beyond 200 °C and triggers active release specifically under high relative humidity or moisture-contact conditions (Atarés & Chiralt, 2016).

Loading EOs into halloysite nanotubes (HNTs), mesoporous silica nanoparticles (MSNs), layered double hydroxides (LDHs), or nanocellulose scaffolds before compounding creates tortuous diffusion pathways that regulate sustained release (Ribeiro-Santos et al., 2017).

Polymer-Essential Oil Combinations, Loading Concentrations, and Property Modifications

When essential oils are dispersed throughout a polymeric network, their low-molecular-weight lipophilic molecules integrate into the macromolecular architecture. This interaction systematically alters the film's mechanical, optical, thermal, and mass transport characteristics.

Physical and Structural Transformations

Incorporating EOs typically decreases tensile strength (TS) and Young's modulus, accompanied by increased elongation at break (EAB). The low-molecular-weight oil droplets position themselves between adjacent macromolecular chains, increasing free volume and polymer chain mobility while decreasing the density of intermolecular hydrogen or dipole-dipole bonds (Atarés & Chiralt, 2016).

Excessive oil loading, however, can induce macroscopic phase separation, creating internal structural discontinuities that embrittle the matrix and lower both TS and EAB. Because essential oils are

hydrophobic, they reduce the film's affinity for water, which can lower water vapor sorption (Ghasemlou et al., 2013).

Oil droplet incorporation can disrupt polymer-network cohesion, generating micro-voids, interfacial defects, and cracks along polymer-lipid phase boundaries. In hydrophilic hydrocolloid films (e.g., chitosan, starch), these micro-pathways often increase Water Vapor Permeability (WVP) at higher loadings (Atarés & Chiralt, 2016).

Non-polar gases like O_2 diffuse more readily through non-polar lipid micro-domains. As a result, EO addition often moderately increases OTR, though the strong radical-scavenging activity of migrating volatiles can offset this effect and help preserve oxidation-sensitive foods (Ribeiro-Santos et al., 2017).

Aromatic rings and conjugated double bonds within EOs (e.g., cinnamaldehyde, eugenol, thymol) strongly absorb light in the UV-C and UV-B regions (200–350 nm). This light-blocking effect helps protect light-sensitive nutrients and lipids from photo-oxidation. At the same time, internal light scattering at the interfaces of dispersed oil droplets increases film opacity and haze while reducing luminous transparency (Ghasemlou et al., 2013).

Shifts in glass transition temperature (Tg) provide thermodynamic evidence of plasticization. In some semicrystalline polymers, high-temperature crystallization behaviors change as finely dispersed nanodroplets act as nucleating agents (Atarés & Chiralt, 2016).

Table 1 summarizes systematically investigated polymer–EO formulations, detailing incorporation loadings, processing methodologies, material property alterations, and functional preservation outcomes.

Polymeric Base Matrix	Essential Oil / Active Constituent	Loading Range	Processing Methodology	Impact on Physical, Mechanical & Barrier Properties	Functional Antimicrobial & Antioxidant Outcomes	Target Food System / Preservation Target
Chitosan (Biopolymer; Cationic Polysaccharide)	Oregano (*Origanum vulgare*) Essential Oil	0.5% – 2.0% (v/v film dope)	Solution Casting (Tween 80 surfactant)	• TS decreases by 28–45% • *EAB* increases significantly • Film opacity increases • WVP increases due to interfacial voids	• Complete growth inhibition of *Listeria monocytogenes* and *E. coli* • Strong radical scavenging (DPPH >80%)	Fresh beef cuts, poultry meat, refrigerated storage
Chitosan	Clove (*Syzygium*	1.0% – 3.0% (w/w	Solution Casting	• Enhanced UV light-	• Strong inhibition of *Staphylococ*	Fresh seafood, salmon

Polymeric Base Matrix	Essential Oil / Active Constituent	Loading Range	Processing Methodology	Impact on Physical, Mechanical & Barrier Properties	Functional Antimicrobial & Antioxidant Outcomes	Target Food System / Preservation Target
	aromaticum) EO / Eugenol	biopolymer)		blocking capacity • Slight yellowish coloration • Moderate increase in film flexibility	*cus aureus* and *Pseudomonas fluorescens* • Retards lipid peroxidation	fillets, pork patties
Poly(lactic acid) (PLA) (Biodegradable Polyester)	Thymol / Carvacrol (Synthetic or isolated fractions)	2.5% – 10.0% (wt/wt)	Melt Compounding & Twin-Screw Extrusion	• T_g drops from 60°C down to 48°C (plasticization) • TS decreases by ~30%	• Substantial vapor-phase activity against *Salmonella enterica* and *Campylobacter jejuni*	Fresh-cut melons, strawberries, bakery goods

Polymeric Base Matrix	Essential Oil / Active Constituent	Loading Range	Processing Methodology	Impact on Physical, Mechanical & Barrier Properties	Functional Antimicrobial & Antioxidant Outcomes	Target Food System / Preservation Target
				• Moderate increase in OTR and WVP	• Controlled sustained release	
Poly(lactic acid) (PLA)	Cinnamon (*Cinnamomum verum*) Bark Oil / Cinnamaldehyde	5.0% – 12.0% (wt/wt)	Electrospinning (Nanofibrous non-woven mats)	• Ultrafine fiber architecture ($d \approx$ 200--450 nm) • Exceptionally high surface area • High encapsulation yield (>80%)	• Fast vapor release inhibiting *Aspergillus niger* and *Penicillium* molds • Doubles fungal shelf life	White bread slices, soft cheeses, bakery products

Polymeric Base Matrix	Essential Oil / Active Constituent	Loading Range	Processing Methodology	Impact on Physical, Mechanical & Barrier Properties	Functional Antimicrobial & Antioxidant Outcomes	Target Food System / Preservation Target
Low-Density Polyethylene (LDPE) (Synthetic Polyolefin)	Rosemary (*Rosmarinus officinalis*) Extract / Carnosic Acid + EO	2.0% – 6.0% (wt/wt)	Twin-screw compounding with Masterbatch blown film	• Minimal loss in tensile strength (<10%) • Negligible change in WVTR • High industrial line speed maintained	• Primary active mechanism: radical scavenging and antioxidant release • Reduces hexanal formation by >60%	High-fat cooked meats, retail meat packaging
Thermoplastic Starch (TPS) (Bio-based Polysaccharide)	Lemongrass (*Cymbopogon citratus*) EO	1.0% – 3.0% (wt/wt starch)	Extrusion & Compression Molding (Glycerol plasticizer)	• Induces phase separation at >2% • TS drops from 8.2	• Broad-spectrum inhibition against *Bacillus*	Table grapes, cherry tomatoes, post-

Polymeric Base Matrix	Essential Oil / Active Constituent	Loading Range	Processing Methodology	Impact on Physical, Mechanical & Barrier Properties	Functional Antimicrobial & Antioxidant Outcomes	Target Food System / Preservation Target
				MPa to 3.8 MPa • UV transmission decreases by >85%	*cereus* and coliforms • Reduces weight loss and decay rate	harvest fruit
Poly(butylene adipate-co-terephthalate) (PBAT)	Tea Tree (*Melaleuca alternifolia*) Oil / Terpinen-4-ol	3.0% – 8.0% (wt/wt)	Melt Blown Film Extrusion	• EAB maintained above 450% • Good sealing performance • Structural integrity preserved	• Substantial antifungal efficacy against gray mold (*Botrytis cinerea*) • Retards enzymatic browning	Fresh mushrooms, delicate berries

Polymeric Base Matrix	**Essential Oil / Active Constituent**	**Loading Range**	**Processing Methodology**	**Impact on Physical, Mechanical & Barrier Properties**	**Functional Antimicrobial & Antioxidant Outcomes**	**Target Food System / Preservation Target**
Gelatin / Whey Protein Isolate (WPI) (Protein Matrices)	Thyme (*Thymus vulgaris*) Essential Oil	0.5% – 2.0% (v/v dope)	Emulsion Casting (Ultrasonic emulsification)	• Droplet diameter < 150 nm increases transparency • Elastic modulus decreases • Water solubility decreases	• High radical scavenging capability (ABTS, DPPH) • Lowers microbial populations by 2–3 log CFU/g	Cold-smoked fish, refrigerated cheese portions

Table 1. Studies based on the use of essential oils in various polymer matrices.

Multifunctional "Smart" Packaging (Active–Intelligent Hybrids)

Integrating active (shelf-life extension) and intelligent (real-time freshness sensing) functions is an expanding research front in food packaging. Modern bio-nanocomposite films integrate essential oils alongside natural pH-sensitive chromophoric indicators (e.g., anthocyanins, curcumin, betalains, alizarin).

Volatile essential oils inhibit bacterial spoilage and oxidation. Concurrently, as food spoilage initiates, basic nitrogenous compounds (Total Volatile Basic Nitrogen - TVB-N: ammonia, dimethylamine, trimethylamine) are generated by surviving flora or endogenous enzymes.

The pH elevation alters the conjugated resonance structure of the co-entrapped anthocyanins, producing a visible color transition (e.g., from red/purple to green/yellow). This provides consumers and supply chain managers with a non-destructive visual readout of food freshness alongside active protection (Dainelli et al., 2008).

Stimuli-Responsive and On-Demand Release Nanotechnologies

Conventional active films frequently release active agents via simple Fickian diffusion immediately upon sealing, which can exhaust the preservative capacity before the food enters its critical spoilage phase. Emerging research focuses on stimuli-responsive packaging that triggers EO release only upon specific environmental changes:

Polymeric films incorporating cyclodextrin-inclusion complexes or hydrophilic nanogels remain chemically dormant in dry states. When humid food products (e.g., fresh-cut fruits, raw meats) generate high headspace water activity (α_w>0.85), water molecules displace the

hydrophobic EO guests from the cyclodextrin cavities, triggering release during periods of high spoilage risk (Atarés & Chiralt, 2016).

Core-shell nanocapsules synthesized with lipid, starch, or protein coatings degrade selectively in the presence of bacterial extracellular enzymes (e.g., lipases, amylases, proteases), releasing EOs in proportion to local microbial concentration (Donsì & Ferrari, 2016).

Polymer matrices designed to swell or contract under fluctuating pH regimes, regulating internal pore diameters to release active volatiles as food acidifies or alkalinizes.

Synergistic Multi-Component Formulations and Aroma Masking

To bypass the strong organoleptic impacts of single essential oils, research has turned to synergistic natural blends. Binary combinations of carvacrol and thymol, or eugenol and cinnamaldehyde, exhibit Fractional Inhibitory Concentration Indices (FICI) <0.5, indicating significant synergy (Bassolé & Juliani, 2012). This allows lower total active concentrations to achieve target antimicrobial thresholds, minimizing sensory disruption.

Pairing volatile EOs with non-volatile active compounds (e.g., nisin, bacteriocins, lysozyme, zinc oxide nanoparticles, silver nanoparticles, green tea polyphenols) produces multi-target preservation mechanisms that suppress both surface-adsorbed and vapor-accessible spoilage organisms (Atarés & Chiralt, 2016).

Toxicological Safety, Migration Kinetics, and Regulatory Landscapes

Before commercial adoption, EO-functionalized active materials must meet regional food contact regulations. While most essential oils and their isolated constituents have GRAS or approved flavoring status in direct food usage, their explicit deployment within packaging

requires verification that migration into the food matrix does not exceed established Specific Migration Limits (SML) or Overall Migration Limits (OML) (typically 10 mg/dm^2 of packaging surface or 60 mg/kg of food simulant) (Ribeiro-Santos et al., 2017).

Consumer acceptance testing remains a primary gatekeeper. Research protocols require trained sensory panels to evaluate whether volatile transfer to sensitive food matrices (e.g., milk, mild cheeses, fresh poultry) alters the baseline aroma and flavor profile (Atarés & Chiralt, 2016).

Conclusions

Integrating essential oils into polymeric packaging networks offers a functional alternative to synthetic chemical preservatives, directly addressing consumer demand for clean-label, sustainable food systems. The shift from traditional, passive barrier packaging to bio-functional active materials provides targeted antimicrobial and antioxidant action at the package interface and within the internal headspace.

While laboratory research confirms the preservation efficacy of these active films, broader commercial implementation requires resolving key engineering hurdles, as follows.

Minimizing thermal degradation and volatile stripping during melt extrusion. Developing affordable nanoencapsulation techniques to modulate release kinetics. Balancing mechanical, optical, and water vapor barrier requirements. Designing multi-component active formulations to mitigate sensory and organoleptic impacts.

Addressing these technical challenges through scalable materials engineering, along with clear regulatory verification and migration modeling, will position essential-oil-functionalized polymers as key

contributors to global food waste reduction and sustainable packaging systems (Ribeiro-Santos et al., 2017).

References

Al-Hassan, A. A., & Norziah, M. H. (2012). Starch–gelatin edible films: Water vapor permeability and mechanical properties as affected by plasticizers. Food Hydrocolloids, 26(1), 108–117. https://doi.org/10.1016/j.foodhyd.2011.04.015

Atarés, L., & Chiralt, A. (2016). Essential oils as additives in active food packaging: A review. Trends in Food Science & Technology, 48, 51–62. https://doi.org/10.1016/j.tifs.2015.12.001

Bakkali, F., Averbeck, S., Averbeck, D., & Idaomar, M. (2008). Biological effects of essential oils—A review. Food and Chemical Toxicology, 46(2), 446–475. https://doi.org/10.1016/j.fct.2007.09.106

Bassolé IH, Juliani HR. Essential oils in combination and their antimicrobial properties. Molecules. 2012 Apr 2;17(4):3989-4006. doi: 10.3390/molecules17043989.

Bentayeb, K., Rubio, C., Batlle, R. et al. Direct determination of carnosic acid in a new active packaging based on natural extract of rosemary. Anal Bioanal Chem 389, 1989–1996 (2007). https://doi.org/10.1007/s00216-007-1570-y

Burt, S. (2004). Essential oils: Their antibacterial properties and potential applications in foods—A review. International Journal of Food Microbiology, 94(3), 223–253. https://doi.org/10.1016/j.ijfoodmicro.2004.03.022

Dainelli, D., Gontard, N., Spyropoulos, D., Zondervan-van den Beuken, E., & Liu, P. (2008). Active and intelligent packaging: Dynamic systems for safe and higher quality food packaging. Trends in Food Science & Technology, 19, S103–S112. https://doi.org/10.1016/j.tifs.2008.09.011

Dhifi, W., Bellili, S., Jazi, S., Bahloul, N., & Mnif, W. (2016). Essential oils' chemical characterization and investigation of some biological activities: A critical review. Medicines, 3(4), Article 25. https://doi.org/10.3390/medicines3040025

Donsì, F., & Ferrari, G. (2016). Essential oil nanoemulsions as antimicrobial agents in food. Journal of Biotechnology, 233, 106–120. https://doi.org/10.1016/j.jbiotec.2016.07.005

European Commission. (2026). Packaging waste. https://environment.ec.europa.eu/topics/waste-and-recycling/packaging-waste_en

Ghasemlou, M., Aliheidari, N., Fahmi, R., Shojaee-Aliabadi, S., Keshavarz, B., Cran, M. J., & Khaksar, R. (2013). Physical, mechanical and barrier properties of corn starch films incorporated with plant essential oils. Carbohydrate Polymers, 98(1), 1117–1126. https://doi.org/10.1016/j.carbpol.2013.07.026

Grand View Research. (2026). *Food packaging market (2026–2033) size, share & trends analysis report* (Report No. GVR-2-68038-365-2). https://www.grandviewresearch.com/industry-analysis/food-packaging-market

Gustavsson, J., Cederberg, C., Sonesson, U., van Otterdijk, R., & Meybeck, A. (2011). *Global food losses and food waste: Extent, causes and prevention*. Food and Agriculture Organization of the United Nations. https://www.fao.org/4/mb060e/mb060e.pdf

Lambert, R. J. W., Skandamis, P. N., Coote, P. J., & Nychas, G. J. (2001). A study of the minimum inhibitory concentration and mode of action of oregano essential oil, thymol and carvacrol. Journal of Applied Microbiology, 91(3), 453–462. https://doi.org/10.1046/j.1365-2672.2001.01428.x

Nazzaro, F., Fratianni, F., De Martino, L., Coppola, R., & De Feo, V. (2013). Effect of essential oils on pathogenic bacteria. Pharmaceuticals, 6(12), 1451–1474. https://doi.org/10.3390/ph6121451

Nerín, C., Tovar, L., Djenane, D., Camo, J., Salafranca, J., Beltrán, J. A., & Roncalés, P. (2006). Stabilization of beef meat by a new active packaging containing natural antioxidants. Journal of Agricultural and Food Chemistry, 54(20), 7840–7846. https://doi.org/10.1021/jf060775c

Petrou, S., Tsiraki, M., Giatrakou, V., & Savvaidis, I. N. (2012). Chitosan dipping or oregano oil treatments, singly or combined on modified atmosphere packaged chicken breast meat. International Journal of Food Microbiology, 156(3), 264–271. https://doi.org/10.1016/j.ijfoodmicro.2012.04.002

Ramos, M., Jiménez, A., Peltzer, M., & Garrigós, M. C. (2012). Characterization and antimicrobial activity studies of polypropylene films with carvacrol and thymol for active packaging. Journal of Food Engineering, 109(3), 513–519. https://doi.org/10.1016/j.jfoodeng.2011.10.031

Ribeiro-Santos, R., Andrade, M., de Melo, N. R., & Sanches-Silva, A. (2017). Use of essential oils in active food packaging: Recent advances and future trends. Trends in Food Science & Technology, 61, 132–140. https://doi.org/10.1016/j.tifs.2016.11.021

Robertson, G. L. (2016). Food packaging: Principles and practice (3rd ed.). CRC Press. https://doi.org/10.1201/b21347

Sadgrove, N., & Jones, G. (2015). A contemporary introduction to essential oils: Chemistry, bioactivity and prospects for Australian agriculture. *Agriculture, 5*(1), 48–102. https://doi.org/10.3390/agriculture5010048

Sanyang, M. L., Sapuan, S. M., Jawaid, M., Ishak, M. R., & Sahari, J. (2016). Development and characterization of sugar palm starch and poly(lactic acid) bilayer films. Carbohydrate Polymers, 146, 36–45. https://doi.org/10.1016/j.carbpol.2016.03.051

Sharifi-Rad, J., Sureda, A., Tenore, G. C., Daglia, M., Sharifi-Rad, M., Valussi, M., Tundis, R., Sharifi-Rad, M., Loizzo, M. R., Ademiluyi, A. O., Sharifi-Rad, R., Ayatollahi, S. A., & Iriti, M. (2017). Biological activities of essential oils: From plant chemoecology to traditional healing systems. *Molecules, 22*(1), 70. https://doi.org/10.3390/molecules22010070

Siracusa, V., Rocculi, P., Romani, S., & Dalla Rosa, M. (2008). Biodegradable polymers for food packaging: A review. Trends in Food Science & Technology, 19(12), 634–643. https://doi.org/10.1016/j.tifs.2008.07.003

Wang, H., Ding, F., Ma, L., & Zhang, Y. (2021). Edible films from chitosan-gelatin: Physical properties and food packaging application. Food Bioscience, 40, Article 100871. https://doi.org/10.1016/j.fbio.2020.100871

Wen, P., Zhu, D.-H., Wu, H., Zong, M.-H., Jing, Y.-R., & Han, S.-Y. (2016). Encapsulation of cinnamon essential oil in electrospun nanofibrous film for active food packaging. Food Control, 59, 366–376. https://doi.org/10.1016/j.foodcont.2015.06.005

Zheng, K., Li, B., Liu, Y., Wu, D., Bai, Y., & Xiang, Q. (2023). Effect of chitosan coating incorporated with oregano essential oil on microbial inactivation and quality properties of refrigerated chicken breasts. *LWT*, *176*, Article 114547. https://doi.org/10.1016/j.lwt.2023.114547


BİDGE